2012

Galaxy Zoo: quantifying morphological indicators of galaxy interaction

Karen Masters
Haverford College, klmasters@haverford.edu

Kevin R.V. Casteels

Steven P. Bamford

Monthly Notices
of the
ROYAL ASTRONOMICAL SOCIETY

MNRAS **429,** 1051–1065 (2013) doi:10.1093/mnras/sts391

Galaxy Zoo: quantifying morphological indicators of galaxy interaction⋆

Kevin. R. V. Casteels,[1,2†] Steven P. Bamford,[2] Ramin A. Skibba,[3] Karen L. Masters,[4,5] Chris J. Lintott,[6,7] William C. Keel,[8] Kevin Schawinski,[9,10‡] Robert C. Nichol[4,5] and Arfon M. Smith[7]

[1]*Departament d'Astronomia i Meteorologia, Universitat de Barcelona, Martí Franques 1, E-08028 Barcelona, Spain*
[2]*School of Physics and Astronomy, The University of Nottingham, University Park, Nottingham NG7 2RD*
[3]*Steward Observatory, University of Arizona, 933 North Cherry Avenue, Tucson, AZ 85721, USA*
[4]*Institute of Cosmology & Gravitation, University of Portsmouth, Dennis Sciama Building, Portsmouth PO1 3FX*
[5]*South East Physics Network§*
[6]*Oxford Astrophysics, Department of Physics, University of Oxford, Denys Wilkinson Building, Keble Road, Oxford OX1 3RH*
[7]*Astronomy Department, Adler Planetarium and Astronomy Museum, 1300 Lake Shore Drive, Chicago, IL 60605, USA*
[8]*Department of Physics & Astronomy, University of Alabama, 206 Gallalee Hall, 514 University Boulevard, Tuscaloosa, AL 35487-0234, USA*
[9]*Department of Physics, Yale University, New Haven, CT 06511, USA*
[10]*Yale Center for Astronomy and Astrophysics, Yale University, PO Box 208121, New Haven, CT 06520, USA*

Accepted 2012 November 11. Received 2012 October 29; in original form 2012 June 21

ABSTRACT

We use Galaxy Zoo 2 visual classifications to study the morphological signatures of interaction between similar-mass galaxy pairs in the Sloan Digital Sky Survey. We find that many observable features correlate with projected pair separation – not only obvious indicators of merging, disturbance and tidal tails, but also more regular features, such as spiral arms and bars. These trends are robustly quantified, using a control sample to account for observational biases, producing measurements of the strength and separation scale of various morphological responses to pair interaction. For example, we find that the presence of spiral features is enhanced at scales $\lesssim 70\,h_{70}^{-1}$ kpc, probably due to both increased star formation and the formation of tidal tails. On the other hand, the likelihood of identifying a bar decreases significantly in pairs with separations $\lesssim 30\,h_{70}^{-1}$ kpc, suggesting that bars are suppressed by close interactions between galaxies of similar mass.

We go on to show how morphological indicators of physical interactions provide a way of significantly refining standard estimates for the frequency of close pair interactions, based on velocity offset and projected separation. The presence of loosely wound spiral arms is found to be a particularly reliable signal of an interaction, for projected pair separations up to $\sim 100\,h_{70}^{-1}$ kpc. We use this indicator to demonstrate our method, constraining the fraction of low-redshift galaxies in truly interacting pairs, with $M_* > 10^{9.5}\,\mathrm{M}_\odot$ and mass ratio <4, to be between 0.4 and 2.7 per cent.

Key words: galaxies: evolution – galaxies: general – galaxies: interactions – galaxies: structure.

1 INTRODUCTION

When galaxies approach one another, their mutual gravitational attraction can result in substantial disruptions to their morphologies, such as tidal arms, counter arms, bridges and tails. Many studies have shown, both analytically and using numerical simulations, that galaxies of similar mass can provoke dramatic disturbances in the stellar distributions of one another, with the details depending on the orbital parameters of the interaction (e.g. Toomre & Toomre 1972; Barnes & Hernquist 1992; Howard et al. 1993; Gerber & Lamb 1994; Barnes 2011). Gravitational perturbations can also redistribute the gas content of galaxies, potentially leading to changes in their star formation properties (e.g. Noguchi 1988; Barnes & Hernquist 1996). These effects are strong functions of pair separation, and hence should be most obvious after the galaxies' first pass, and particularly around times of closest approach. Many

⋆ This publication has been made possible by the participation of more than 200 000 volunteers in the Galaxy Zoo project. Their contributions are acknowledged at http://authors.galaxyzoo.org.
† E-mail: kcasteels@am.ub.es
‡ Einstein Fellow.
§ http://www.sepnet.ac.uk

interactions are ultimately likely to result in the complete morphological transformation of the galaxies involved (e.g. Toomre 1977; Hopkins et al. 2008). However, more subtle effects are expected both earlier, while the galaxies are on their initial approach, and at times of wide separation between passes (e.g. Perez et al. 2006; Lotz et al. 2008; Struck, Dobbs & Hwang 2011).

The expected strength and prevalence of pair interactions mean that they are potentially important for determining the properties and evolution of the galaxy population. It is therefore critical that we test our theoretical expectations of the effects of such interactions by studying representative samples of interacting systems. Furthermore, we may utilize the observed frequency of interacting pairs to discriminate between the details of cosmological galaxy formation models.

A relatively straightforward, and physically motivated, definition of 'interacting' galaxies is a pair for which the tidal force experienced across one of the galaxies, averaged over its internal dynamical time, F_t, is at least some specified fraction of the gravitational force binding the outer regions of that galaxy, F_g. By this definition, all interacting pairs should produce significant internal dynamical effects, which would have otherwise been absent, in at least one of the member galaxies. In practice, however, it is difficult to measure the forces involved. We may estimate them by studying the effects of an interaction, but the relative orientations and types of the galaxies in each pair, as well as observational limitations, lead to large variations in the apparent effects for interactions of a given strength, F_t/F_g.

A more convenient definition, which is roughly equivalent, although only statistically applicable, is that galaxies in a pair are 'interacting' if their gravitational influence upon one another could have observable effects in a favourable orientation and mix of galaxy types. For example, a pair of elliptical galaxies might not display signatures of an interaction in a given observation, but would still count as 'interacting' by this definition if the tidal forces they are experiencing would have been sufficient to produce an observable signature in a pair of spirals. The observational details of a particular data set therefore fix the minimum F_t/F_g probed. This definition removes much of the incompleteness associated with only considering pairs with observational signs of interaction, but of course only a fraction of such 'interacting' galaxies will possess observational signatures. As we shall see later in this paper, it is nevertheless possible to constrain the fraction of galaxies interacting according to this definition.

Studies of galaxy pairs typically discuss close pairs, bound pairs, merging pairs or pairs with observational disturbances, but often mix the usage and definitions of these classes. Interacting pairs are closely related to bound pairs, for which the sum of the gravitational potential energy and kinetic energy of the pair is negative. However, not all interacting pairs are bound, particularly where both are part of a larger system, such as a galaxy cluster. Likewise, not all bound pairs will be experiencing significant tidal interactions. Interacting pairs are also closely related to mergers. Galaxies in bound pairs will typically merge on relatively short time-scales if they are experiencing significant tidal interactions, as the kinetic energy of the pair orbit is transferred to deforming and heating the internal mass distribution of each galaxy (e.g. Struck 1999).

We can identify close pairs of galaxies which are likely to be sufficiently near to one another such that they are interacting (and potentially bound and will eventually merge) using projected distance and line-of-sight velocity (Charlton & Salpeter 1991). However, this approach suffers from significant contamination and incompleteness (with respect to the above definitions of physically meaningful interacting, bound or merging selections), due to a lack of full spatial information and the inverse relationship between relative velocity and separation for loose pairs (i.e. very close pairs can have very large relative peculiar velocities, so appear significantly separated in redshift space). Observational signatures of interactions, for example visual classifications, quantitative morphological measurements or induced star formation, may be used to improve the selection of truly interacting galaxies. However, as often one wishes to study the physical effect of interactions, one must be careful to avoid a circular argument.

The early atlases of Vorontsov-Velyaminov (1959, 1977) and Arp (1966) clearly demonstrated that interactions between galaxies can have profound effects on their morphologies, providing examples of bridges, tails, distorted spiral patterns and other features. These morphological changes were observed between pairs up to over $100\,h_{70}^{-1}$ kpc, as is the case for the bridging filament of Arp 295. The restricted three-body simulations of Toomre & Toomre (1972) clearly demonstrated that these features are the result of strong tidal forces between the interacting galaxies. That galaxy interactions can also induce star formation was first suggested by Larson & Tinsley (1978), who found that the scatter in the *UBV* colours of interacting galaxies from the Arp atlas was significantly larger than normal galaxies from the *Hubble Atlas* (Sandage 1961). Similar evidence for interaction-induced star formation has also been found over a wide range of the energy spectrum, from near-ultraviolet to radio (e.g. Kennicutt & Keel 1984; Keel et al. 1985; Bushouse 1986, 1987; Kennicutt et al. 1987; Hummel et al. 1990).

Studies which use quantitative measures of morphology find signs of interaction at fairly small projected separations. Using the CAS method of Conselice (2003) to measure galaxy asymmetry (A) and concentration (C), Hernández-Toledo et al. (2005) found that both these quantities increase, relative to isolated galaxies, for galaxy pairs with separations less than the photometric diameter of the primary. De Propris et al. (2007) reliably identified interacting pairs with projected separations up to $r_p \lesssim 50\,h_{70}^{-1}$ kpc using $A > 0.35$ and visual confirmation, for a sample of pairs with line-of-sight velocity differences $\Delta V < 500\,\mathrm{km\,s^{-1}}$.[1] Similarly, Ellison et al. (2010) show that asymmetry increases for $r_p \lesssim 50\,h_{70}^{-1}$ kpc for a sample of pairs with $\Delta V < 200\,\mathrm{km\,s^{-1}}$.

Meanwhile, studies which probe the effects of tidal interaction through star formation modulations find changes up to larger projected separations. Nikolic, Cullen & Alexander (2004) demonstrate an increase in star formation at $r_p \lesssim 70\,h_{70}^{-1}$ kpc for early- and mixed-type pairs, and at $r_p \lesssim 430\,h_{70}^{-1}$ kpc (their maximum separation probed) for late-type pairs. They also find that pairs with $r_p \lesssim 110\,h_{70}^{-1}$ kpc show a strong increase in central concentration, suggestive of nuclear starbursts. Li et al. (2008) find a star formation increase for close pairs, with star formation rate (SFR) enhanced by a factor of 1.5 at $r_p \lesssim 140\,h_{70}^{-1}$ kpc to a factor of 4 at $r_p \lesssim 30\,h_{70}^{-1}$ kpc. This strong dependence on r_p is contrasted with a weak dependence on luminosity ratio, with the star formation enhancement being the strongest in lower luminosity galaxies. Ellison et al. (2008), Robaina et al. (2009) and Patton et al. (2011) all find a strong increase in SFR for $r_p < 40\,h_{70}^{-1}$ kpc, while Patton et al. (2011) also see a smaller increase up to at least $r_p < 80\,h_{70}^{-1}$ kpc (their maximum separation probed) for $\Delta V < 200\,\mathrm{km\,s^{-1}}$ pairs. There is also evidence that equivalent levels of tidally induced star formation require smaller

[1] Throughout this introduction, separations quoted from other studies have been converted to units of h_{70}^{-1} kpc as necessary.

r_p in denser environments (e.g. Lambas et al. 2003; Alonso et al. 2004).

Some of the variation in the separation scale at which different studies begin to see the effects of tidal interactions is likely due to differences in the mass and luminosity ranges of the samples, as well as the methods used. However, it appears clear that the effects of tidal interactions are found at larger projected separations when identified by induced star formation (up to 80–100 h_{70}^{-1} kpc), compared to quantitative measurements of asymmetry (up to $\sim$30 h_{70}^{-1} kpc). This is consistent with the results of Lotz et al. (2008), which used simulations to show that quantitative morphological methods for finding merging galaxies, such as A, Gini and M_{20}, are most sensitive for galaxies undergoing close passages and during the post-merger phase. Induced star formation, on the other hand, will be evident between passes, when the galaxies achieve a wide separation before falling back towards one another, or in galaxies which have experienced a close encounter but will not merge. Note that in dry mergers there may be no star formation signature of the interaction, and morphological features will typically only be observable for short times (Bell et al. 2006).

As mentioned previously, interacting galaxies can produce distinctive morphological features such as tidal arms, counter arms, bridges and tails, which are best classified visually. These features are extremely reliable for discriminating truly interacting galaxies from interlopers in close pair catalogues. Features such as two loosely wound tidal arms may not be detectable by quantitative morphology methods because these galaxies may not appear to be sufficiently asymmetric or disturbed, especially between the first and second pass when the galaxies may appear to be widely separated. One of the advantages of using visual morphological classifications over automated methods is the ability to identify very faint and subtle features. Tidal features are known to become rapidly undetectable as a function of time and survey imaging depth (e.g. Bell et al. 2006; Schawinski et al. 2010); however, we find that the Galaxy Zoo classifications used in this paper are extremely sensitive to faint features. Furthermore, as we will show, by studying the occurrence of such features in a statistical sense, and making weak assumptions concerning the observability of physical interactions, we are able to make decisive statements concerning the prevalence of interactions.

The visual classification of peculiar, disturbed and interacting galaxies has a long history, beginning with Hubble (1926). The catalogues of Vorontsov-Velyaminov (1959, 1977), Sandage (1961) and Arp (1966) complied together a significant number of galaxies with obvious tidal features. Such work continues to be valuable today, for example Bridge, Carlberg & Sullivan (2010) use visual classifications of galactic bridges and tails in the Canada–France–Hawaii Telescope Legacy Survey to study the evolution of the galaxy interaction fraction (GIF) with redshift. These galaxies were either isolated merger remnants or fairly close interacting pairs, due to their requirement that galaxy pairs be connected by a bridge. Nakamura et al. (2003) and Fukugita et al. (2007) visually classified a subsample of $\sim$2500 bright galaxies from the Sloan Digital Sky Survey (SDSS; York et al. 2000) imaging of SDSS galaxy objects, finding that $\sim$1.5 per cent of galaxies in their nearby magnitude-limited sample show morphological indications of interaction. Nair & Abraham (2010) provide an impressive catalogue of detailed visual classifications for over 14 000 bright SDSS galaxies, which includes information regarding tidal tails and other indicators of interaction.

The Galaxy Zoo project has enabled visual classification to be performed for extremely large samples, allowing the continued use of this valuable technique with modern surveys. Skibba et al. (2009) obtained the marked correlation function for the Galaxy Zoo 1 merger classification likelihood and found that it increases sharply in their closest r_p bin (of 170 h_{70}^{-1} kpc width), and found evidence that most of this increase was for pairs with $r_p \lesssim 30\,h_{70}^{-1}$ kpc. Taking an alternative approach, Darg et al. (2010a,b) imposed thresholds to select Galaxy Zoo 1 galaxies with high merger classification likelihoods and study their frequency and properties. Most of these galaxies are either highly disturbed systems or very close pairs. While these studies have been successful at identifying a subset of interacting pairs, they primarily select galaxies which have relatively small projected separations and so do not typically identify interacting pairs which are at large projected separation between their first and second close passes.

In this paper, we use visual classifications from Galaxy Zoo 2 to study what morphological changes are taking place in interacting galaxy pairs as a function of physical projected separation (r_p) and line-of-sight velocity difference (ΔV). We then use these results to estimate the frequency of pair galaxy interactions in the local Universe.

In Section 2 we describe the data set and sample selection, in Section 3 we outline the methods employed, in Section 4 we present our results and in Section 5 we summarize our results and discuss their implications. A Λ cold dark matter cosmology is assumed throughout, with $\Omega_\Lambda = 0.7$, $\Omega_m = 0.3$ and $h_{70} = H_0/(70\,\mathrm{km\,s^{-1}\,Mpc^{-1}})$.

2 GALAXY ZOO 2 DATA AND SAMPLE SELECTION

Although there have been many attempts at completely automating morphological classification, visual inspection remains the preferred method for many astronomers. However, for the large samples produced by modern surveys, visual classification is not feasible for a normal research team to perform in a reasonable time. Galaxy Zoo (Lintott et al. 2008) is an online citizen science project designed to address this problem, by involving large numbers of the public in classifying the morphological features of galaxies. The original Galaxy Zoo web site collected classifications for nearly one million galaxies from SDSS Data Release 6 (DR6; Adelman-McCarthy et al. 2008), which were processed to produce catalogues of visual classifications together with estimates of their accuracy. These data have been released to the public,[2] and are described in Lintott et al. (2011).

The original Galaxy Zoo (GZ1) was limited to coarse morphological classification. Following its success, a subsequent project was launched, this time collecting much more detailed morphological information via a question tree, for a subset of $\sim$300 000 of the brightest galaxies from Galaxy Zoo. This project, named Galaxy Zoo 2 (GZ2), ran from 2009 February 16 until 2010 April 22 and collected 16 340 298 classifications (comprising a total of 58 719 719 questions) by 83 943 participants for 325 651 galaxy images.[3] Both GZ1 and GZ2 used *gri* composite colour images provided by the SDSS, created following the prescription of Lupton et al. (2004). These were displayed such that each galaxy had the same apparent size. See Masters et al. (2011) for additional discussion of the GZ2 data set.

[2] Galaxy Zoo data are publicly available at http://data.galaxyzoo.org/

[3] The GZ2 web site is archived at http://zoo2.galaxyzoo.org

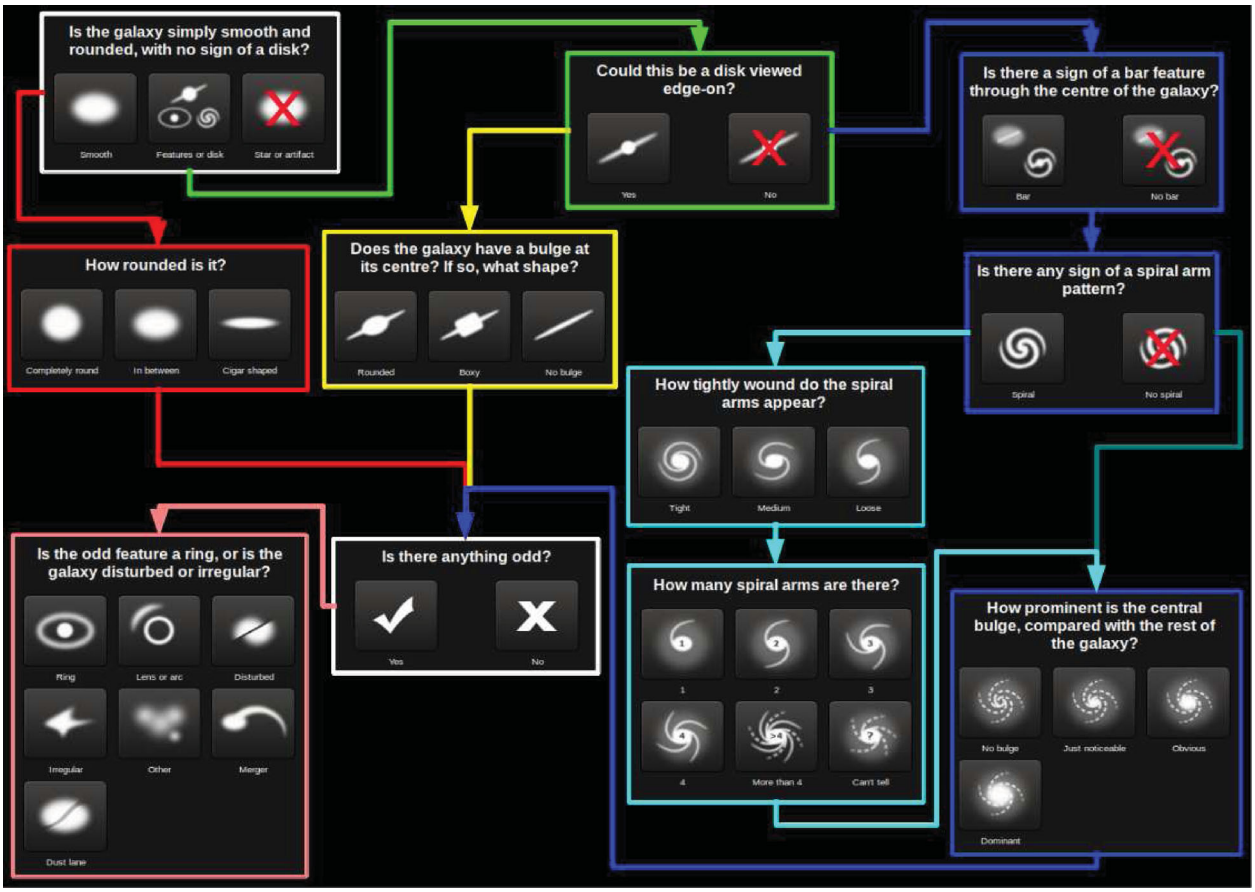

Figure 1. The Galaxy Zoo 2 question tree.

Fig. 1 presents the classification tree used for GZ2, including the actual button images shown to the GZ2 participants. These images attempt to symbolize the answer to each question. Most of the participants have no formal astronomy training and, although there is a tutorial which presents real examples for each answer, it is likely that they rely on these images to a reasonable degree while making their classifications.

The GZ2 sample selection includes 273 783 galaxies from SDSS DR7 with $R_{90} > 3$ arcsec and $r_{\mathrm{Petro,AB}} < 17.0$ and located in the contiguous North Galactic Cap region.[4] In this paper we require redshift information, and therefore restrict our sample to galaxies with spectra in DR7. The overall spectroscopic completeness of this GZ2 sample is 86 per cent. As given in Masters et al. (2010), we limit our sample of galaxies to $z < 0.09$ to ensure sufficient resolution for spiral classifications and thereby reduce somewhat the redshift classification bias discussed in Bamford et al. (2009). A lower redshift limit of $z > 0.01$ is imposed to avoid the de-blending of large nearby objects into multiple photometric objects by the SDSS pipeline, and ensure that redshift-derived distance moduli are sufficiently accurate. Applying these limits results in a sample of 148 291 galaxies.

We make use of the Max-Plank-Institute for Astrophysics - Johns Hopkins University (MPA-JHU) DR7 median stellar mass measurements,[5] which are based on fits to the SDSS photometry, following the methods of Kauffmann et al. (2003) and Salim et al. (2007).

3 METHOD

3.1 Pair and control samples

In this study, we focus on galaxy pairs with stellar mass ratios between 1:1 and 4:1. These would amount to major mergers, if the interaction were to proceed that far. The candidate galaxy pairs in our parent sample are selected to have an absolute line-of-sight velocity difference of $\Delta V < 5000\,\mathrm{km\,s^{-1}}$ and a physical projected separation (converted from an angular separation using the average redshift of the pair) of $r_{\mathrm{p}} < 1000\,h_{70}^{-1}$ kpc.

To probe the effects of changing ΔV between pairs we divide our sample into $100\,\mathrm{km\,s^{-1}}$ bins for $\Delta V < 500\,\mathrm{km\,s^{-1}}$, as well as two larger ΔV bins with $500 < \Delta V < 1000$ and $1000 < \Delta V < 5000\,\mathrm{km\,s^{-1}}$. The $1000 < \Delta V < 5000\,\mathrm{km\,s^{-1}}$ pairs serve as our control sample, as they should all be physically unassociated. These are used to account for biases that result in a dependence of some morphological classifications on the projected separation of galaxies, irrespective of any true interaction. They also indicate the typical

[4] GZ2 also included ∼30 000 galaxies from both the normal- and co-add-depth imaging of the SDSS Stripe 82 region, but these data are not used in this paper.

[5] This catalogue is publicly available at http://www.mpa-garching.mpg.de/SDSS/DR7/Data/stellarmass.html

level of morphological features present in the general galaxy population, for comparison with our pair samples.

Note that pairs with $\Delta V > 5000\,\mathrm{km\,s^{-1}}$ have a significantly different luminosity distribution (skewed to more luminous galaxies) compared to the lower ΔV samples. This is a result of ΔV approaching the velocity range of the survey, and hence the sample becoming dominated by more distant, intrinsically brighter galaxies. We judge the $1000 < \Delta V < 5000\,\mathrm{km\,s^{-1}}$ range to be a good compromise between maintaining consistent luminosity selections, while maximizing the control sample size and minimizing its contamination by physically associated pairs.

3.2 Morphology probabilities

GZ2 participants are asked a series of questions for each image, with each answer determining the subsequent question, as depicted in Fig. 1. We record the individual answers provided and, after some down-weighting of the most inconsistent participants, use these to construct a catalogue. This catalogue gives the total number of times each galaxy was presented and, for each question, the fraction of votes for each possible answer, which we denote $f(A)$. The $f(A)$ for all A belonging to a single question must, of course, sum to unity. To give a concrete example, consider that a given galaxy has been presented to 20 participants, 16 of which answered 'Features or disc' to the initial question 'Is the galaxy simply smooth and rounded, with no sign of a disc?'. This galaxy thus has a vote fraction of $f(\mathit{Features}) = 0.8$. The 16 participants who answered *Features* were then asked 'Could this be a disc viewed edge-on?', with 12 answering 'No', and thus $f(\mathit{Edge\text{-}on} = \mathit{No}) = 0.75$. All these 12 were subsequently asked 'Is there a sign of a bar feature through the centre of the galaxy?', resulting in a split of $f(\mathit{Bar} = \mathit{Yes}) = 0.5$ and $f(\mathit{Bar} = \mathit{No}) = 0.5$. Again, all 12 were then asked 'Is there any sign of a spiral arm pattern?', with a 'Yes' answer fraction of $f(\mathit{Spiral} = \mathit{Yes}) = 0.75$. The question tree continues, and we have only considered the route through the question tree taken by the majority, but this is sufficient for the reader to fully understand both the traversal of the question tree and the definition of $f(A)$.

The vote fraction $f(A)$ may, very roughly, be considered to represent probabilities regarding a galaxy's morphology. The uncertainty expressed by these probabilities results from a combination of limited observational information, true morphologies which do not precisely align with the possible answers, and differing interpretations by each participant in judging the correspondence between the image and each answer. In this case $f(A) = p(A|\boldsymbol{M})$, the conditional probability of the galaxy having morphological feature A given that it possesses the set of morphological features $\boldsymbol{M}$, since each participant must have identified the galaxy as having the preceding features in the question tree, $\boldsymbol{M}$, in order to be asked about feature A.

The conditional probability compares the likelihood of a galaxy having feature A against the alternative answers for a single question. However, it does not necessarily give a good representation of the presence of a particular morphological feature. An object may have a high $f(A)$, but still be unlikely to possess morphological attribute A. To assess the overall likelihood of A, one may calculate an estimate for the joint probability of A and $\boldsymbol{M}$. Formally, this is

$$p(A \cap \boldsymbol{M}) = p(A|\boldsymbol{M})\, p(\boldsymbol{M}) \tag{1}$$

$$= f(A) \prod_{\boldsymbol{Q} \subset \boldsymbol{M}} \sum_{a \in \boldsymbol{Q}} f(a)\,, \tag{2}$$

where $\boldsymbol{Q}$ are subsets of the set of answers $\boldsymbol{M}$ partitioned by question, and the a are the individual answers in $\boldsymbol{Q}$.

As we do not distinguish between the different paths which lead to a given question (though this would be possible to do from the raw data), we only consider cases for which $\boldsymbol{M}$ represents the sum of all possible paths to answer A. In this case, we denote $p(A) = p(A \cap \boldsymbol{M})$, where $p(A)$ is the probability of morphological feature A together with any $\boldsymbol{M}$ for which asking the question with answer A is relevant, as defined by the question tree in Fig. 1. Remember that these probabilities only include the observational information available in GZ2, so do not necessarily equate to the true probability of a particular morphology feature. For example, for a galaxy which has $f(\mathit{Features} = \mathit{Yes}) < 1$ or $f(\mathit{Edge\text{-}on} = \mathit{No}) < 1$, the value of $p(\mathit{Spiral} = \mathit{Yes})$ does not take into account the unobservable (in terms of GZ2) presence of spiral arms in apparently smooth or edge-on galaxies.

For the example above,

$$p(\mathit{Spiral} = \mathit{Yes} \mid \mathit{Features} \cap \mathit{Edge\text{-}on} = \mathit{No}) = f(\mathit{Spiral} = \mathit{Yes}) = 0.75\,, \tag{3}$$

whereas

$$\begin{aligned} &p(\mathit{Spiral} = \mathit{Yes}) \\ &= p(\mathit{Spiral} = \mathit{Yes} \cap \mathit{Features} \cap \mathit{Edge\text{-}on} = \mathit{No}) \\ &= f(\mathit{Spiral} = \mathit{Yes})\, f(\mathit{Edge\text{-}on} = \mathit{No})\, f(\mathit{Features}) = 0.45\,. \end{aligned} \tag{4}$$

This indicates that there is only a moderate probability that the object in question has visible spiral arms, although if one is willing to accept that it does have features and is not edge-on, then it probably does possess spiral arms. Note that the *Bar* question has been implicitly omitted from this calculation as all its possible answers continue on to the *Spiral* question, and hence it would contribute a factor of $[f(\mathit{Bar} = \mathit{Yes}) + f(\mathit{Bar} = \mathit{No})] = 1$.

Whether one works with $f(A)$ or $p(A)$ depends upon the question one is considering. It is particularly useful to examine trends in terms of $f(A)$ itself, as this reflects the behaviour of a specific morphological feature, irrespective of other morphological variations. However, due to the limited total number of times each object is considered, when $p(A)$ is low, $f(A)$ will be highly quantized and subject to high Poisson noise. In this case, one can consider only objects for which $f(A)$ is meaningful, by imposing a minimum threshold on $p(\boldsymbol{M})$, which we denote by $f(A \mid p(\boldsymbol{M}) > t)$, for some threshold t.

To study the dependence of $f(A)$ on projected separation (r_p) for a particular sample, we take the mean vote fraction $f(A)$ in each bin of r_p,

$$f(r_\mathrm{p}, A) = \frac{1}{N} \sum_{i=1}^{N} f(A)_i\,, \tag{5}$$

where the sums are over the N galaxies in each r_p bin for that sample. This is done for each of the answers, A, shown in Fig. 1.

For many answers, we find that the control sample displays a dependence on r_p. Given their velocity separation, these trends cannot be due to any physical interactions within the pairs. Instead they must arise from the apparent close projection of the galaxies, and may be considered to be a 'projection bias', which will contaminate any signature of physical interaction in the lower ΔV pairs. In order to remove this contamination, we remove the control sample trends versus r_p from the observed trends for the other pair samples. If we regard the $f(r_\mathrm{p}, A)$ as conditional probabilities, the control sample trend may be removed by

$$F = (f_\mathrm{p} - f_\mathrm{c}) / (1 - f_\mathrm{c})\,, \tag{6}$$

where F is the conditional probability in the absence of the projection bias, $f_{\rm p}$ is the measured conditional probability for a sample of physically associated pairs and $f_{\rm c}$ is the measured conditional probability for the control sample. $F(r_{\rm p}, A)$ therefore represents the conditional probability, $P(r_{\rm p}, A|\boldsymbol{M})$, of morphological feature A being observed as a result of the galaxy being in a pair with separation $r_{\rm p}$, given that the galaxy displays morphological features $\boldsymbol{M}$.

The uncertainties on $F(r_{\rm p}, A)$ are given by

$$\sigma_F^2 = \frac{(1-f_{\rm p})^2}{(1-f_{\rm c})^4}\,\sigma_{f_{\rm c}}^2 + \frac{1}{(1-f_{\rm c})^2}\,\sigma_{f_{\rm p}}^2\,, \tag{7}$$

where $\sigma_{f_{\rm c}}$ and $\sigma_{f_{\rm p}}$ are determined from the standard error of $f_{\rm c}$ and $f_{\rm p}$ in each $r_{\rm p}$ bin.

Note that for physically associated pairs, with low ΔV, the projected galaxy density increases as $r_{\rm p}$ decreases, such that the number of galaxies in a given $r_{\rm p}$ bin, and hence the signal-to-noise ratio of $f(r_{\rm p}, A)$, remains reasonably constant. However, for unassociated pairs the projected galaxy density is constant as a function of $r_{\rm p}$, and thus at small $r_{\rm p}$ the signal-to-noise ratio of $f(r_{\rm p}, A)$ drops substantially. Unfortunately, this limits the accuracy of the projection bias correction and translates into higher uncertainties in $F(r_{\rm p}, A)$ at low $r_{\rm p}$.

In order to quantify the strength and scale of the trends, we fit the $F(r_{\rm p}, A)$ with the function

$$F(r_{\rm p}) = a\exp(-r_{\rm p}/b) + c\,, \tag{8}$$

where a is the size of the change in F from large to small r, b specifies the r scale of the trend and c accounts for possible constant systematic offsets between the physically associated pairs and control sample. We find that this simple empirical function is able to well represent most of the $F(r_{\rm p})$ trends we observe. Ideally c should be zero, and in any case, for $F(r_{\rm p})$ to represent a probability, $0 < c < (1-a)$. However, systematic offsets of c in either direction are possible due to small differences in the sample selections of physically selected pairs and the control sample. These are difficult to avoid for different ΔV selections, but should not have an $r_{\rm p}$ dependence, justifying the use of a simple constant to account for them. Reassuringly, we find that c is generally very close to zero, signifying that sample selection differences are indeed minimal. The fitting method provides uncertainties on a, b and c, which enables us to judge the significance of differences in the trends between samples and plot confidence intervals on the fitting functions.

3.3 Counting companions

In Section 4.6, we study the number of close companions per galaxy as a function of projected separation, $N_{\rm c}(r_{\rm p})$, for a mass-limited sample. Following the methods of Patton et al. (2000, 2002), weights are applied to account for pairs near the survey boundaries (w_{b_2}), pairs near the redshift boundaries (w_{v_2}), global spectroscopic incompleteness weights (w_s), as well as angular spectroscopic incompleteness weights to correct for fibre collisions at small angular separation (w_{θ_2}). The uncertainties in these weights are determined primarily from uncertainties in the astrometric and redshift measurements. Because the uncertainties in the pair statistics obtained in Section 4.6 are significantly larger than the astrometric and redshift uncertainties, uncertainties are not explicitly calculated for these weights.

In Section 4.6, we will derive an additional weight ($w_{\rm int}$) to account for the occurrence of interlopers: galaxies in close pairs (as judged by $r_{\rm p}$ and ΔV), but which are not truly interacting. Previous studies typically ignore this, or estimate a constant value, whereas we will derive its dependence on $r_{\rm p}$.

The total weight assigned to each galaxy is thus

$$w_{N_2} = w_s^2\, w_{\theta_2}\, w_{b_2}\, w_{v_2}\, w_{\rm int}\,. \tag{9}$$

The total number of companion galaxies of host galaxy i, with projected separation $r_{\rm p}$, is given by summing these weights for all companions within a given projected separation

$$N_{{\rm c},i}(r_{\rm p}) = \sum_{j=1}^{N} R(r_{{\rm p},j})\, w_{N_2,j}\,, \tag{10}$$

where N is the total number of galaxies in the sample and $R(r) = 1$ if r is in the current $r_{\rm p}$ bin, and 0 otherwise.

The average number of close companions per galaxy, as a function of projected separation, is then calculated as the mean of the number of companions of each galaxy, weighted by the spectroscopic incompleteness:

$$N_{\rm c}(r_{\rm p}) = \frac{1}{N w_{\rm s}} \sum_{i=1}^{N} N_{{\rm c},i}(r_{\rm p})\,. \tag{11}$$

For $N_{\rm c}(r_{\rm p}) \ll 1$, this is equivalent to the fraction of galaxies with close companions.

4 RESULTS

Following the method described in Section 3.2, we have examined all of the GZ2 answers to ascertain which are most relevant to studying galaxy interactions. The questions which are of most interest for this paper are those regarding odd features, bars, the spiral arm winding tightness and the number of spiral arms. As can be seen in Fig. 1, for each object every participant is asked 'Is there anything odd?' and, if they answer 'Yes', asked to specify one odd feature from seven alternatives. In order for a participant to be asked the questions regarding spiral arm number and winding tightness, they must answer *Features*, *Edge-on=No* and *Spiral=Yes* in the preceding set of questions.

In Sections 4.1, 4.2, 4.3 and 4.4, we use the bias-corrected vote fractions, $F(r_{\rm p}, A)$, corresponding to the probability of galaxy property A occurring as a result of the galaxy being in a pair with separation $r_{\rm p}$. For example, $F(r_{\rm p}, \mathit{1\,Arm}) = P(r_{\rm p}, \mathit{1\,Arm} \,|\, \mathit{Features} \cap \mathit{Edge\text{-}on} = \mathit{No} \cap \mathit{Spiral} = \mathit{Yes})$. We use the full sample, without applying any thresholds for the preceding questions, in order to see what classification trends exist for that morphological feature in relation to pair separation irrespective of other morphological features.

In Sections 4.5 and 4.6, we select individual galaxies based on their morphological features, and wish to minimize the impact of noisy $f(A)$ values for galaxies with low $p(A)$. We therefore impose a threshold on $p(A)$ to select only objects for which asking the question with answer A is likely to be appropriate.

4.1 The Odd class

In Fig. 2, we study the trends in 'Odd' GZ2 morphologies as a function of pair separation. The main panels plot the mean vote fraction, $F(r_{\rm p}, A)$, of $\Delta V < 500\,{\rm km\,s^{-1}}$ close pairs, correcting for projection bias effects using the $1000 < \Delta V < 5000\,{\rm km\,s^{-1}}$ control sample, as outlined in Section 3.2. This may be interpreted as the probability, $P(r_{\rm p}, A|\boldsymbol{M})$, of a galaxy in this sample displaying the specified morphological attribute, purely as a result of being in a pair with separation $r_{\rm p}$. The raw vote fractions, $f(r_{\rm p}, A)$, from which the corrected quantities are determined, are also shown in the inset panels.

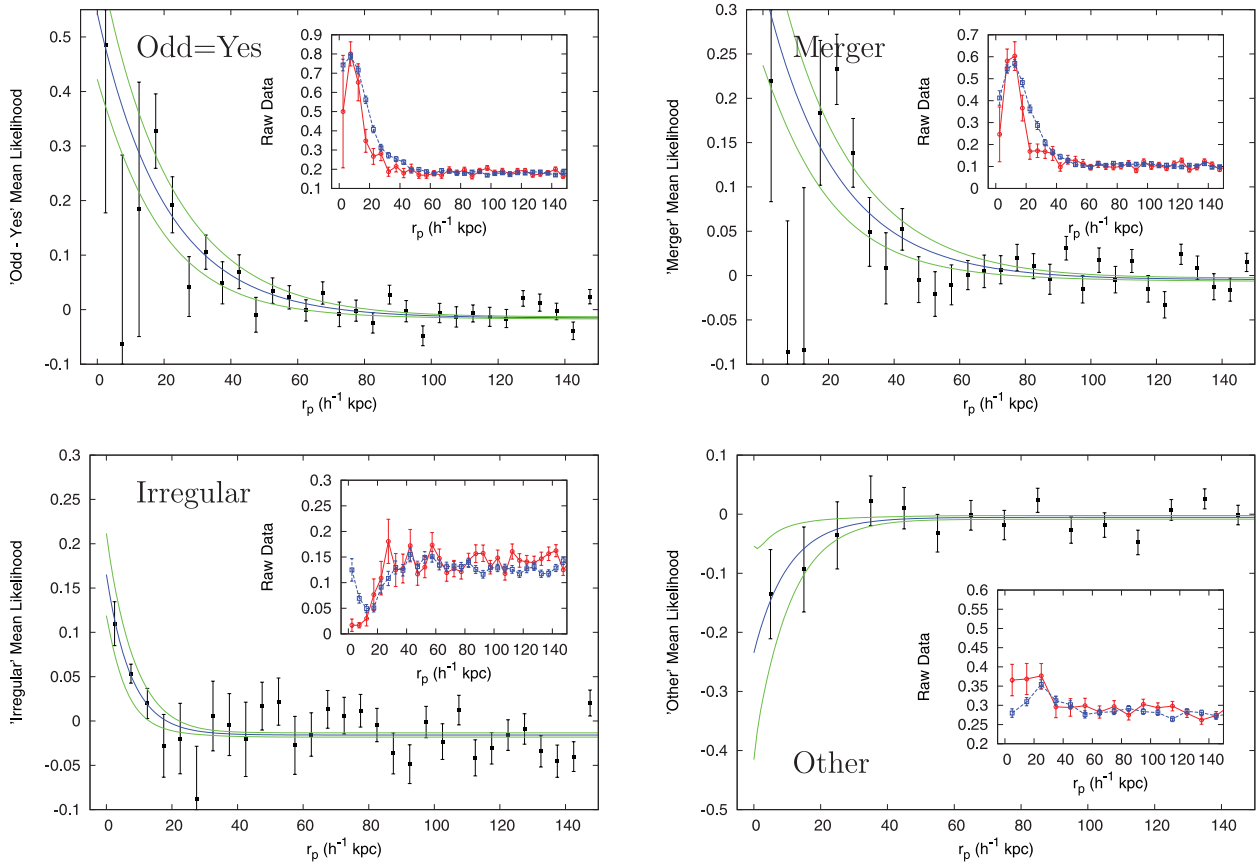

Figure 2. Mean vote fractions for the *Odd=Yes* answer and subsequent 'odd' categories which show trends versus r_p: *Merger*, *Irregular* and *Other*. The main plot in each panel shows the mean vote fraction of $\Delta V < 500\,\mathrm{km\,s^{-1}}$ close pairs, corrected for projection bias, i.e. $F(r_p, A) = P(r_p, A|\boldsymbol{M})$ (points with error bars), together with best fit (blue line) to these points using equation (8) and the corresponding 1σ confidence region (green lines). The insets plot $f(r_p, A)$ for the $\Delta V < 500\,\mathrm{km\,s^{-1}}$ close pairs (blue) and $1000 < \Delta V < 5000\,\mathrm{km\,s^{-1}}$ control sample pairs (red), from which $F(r_p, A)$ is calculated.

Considering first the *Odd=Yes* answer itself, the top left-hand panel in Fig. 2, we see from the inset plot that the raw vote fractions, $f(r_p, Odd = Yes)$, increase strongly with decreasing r_p for both the $\Delta V < 500\,\mathrm{km\,s^{-1}}$ close pairs and the control sample. As the pairs in the control sample are physically unassociated, this indicates that GZ2 participants identified some galaxies as 'Odd' simply as a result of their apparent separation. This projection bias strongly contaminates the $f(r_p, Odd = Yes)$ results of the $\Delta V < 500\,\mathrm{km\,s^{-1}}$ close pair sample. However, there are offsets between the $f(r_p, Odd = Yes)$, such that the $\Delta V < 500\,\mathrm{km\,s^{-1}}$ close pairs are more likely to be marked 'Odd' than the control sample, particularly at $20 \lesssim r_p \lesssim 40\,h_{70}^{-1}$ kpc.

Indeed, when we correct for the projection bias, we see clear evidence for a trend. GZ2 participants were more likely to identify an object as 'Odd' if it is in a $\Delta V < 500\,\mathrm{km\,s^{-1}}$ close pair with small projected separation. The probability of a galaxy being labelled 'Odd', as a result of being in a pair, $P(Odd = Yes)$, varies from zero for $r_p \gtrsim 80\,h_{70}^{-1}$ kpc to ~0.5 for the smallest projected separations. The empirical function defined in equation (8) does a good job of representing this trend.

If a participant answered *Odd=Yes*, they were then asked to identify the odd feature more precisely by selecting one option from a variety of possibilities. The remaining panels of Fig. 2 plot $F(r_p, A) = P(r_p, A \,|\, Odd = Yes)$ for three of these options. From the top right-hand panel of Fig. 2, we see that the *Merger* answer mimics the behaviour of *Odd=Yes*, although note that we are plotting the conditional probability given that the object does display an 'Odd' feature, and hence the *Odd=Yes* behaviour itself is not included in this quantity.

We see, from the raw vote fractions, that the *Merger* answer is strongly dependent on the apparent separation of galaxy pairs. Galaxies are often marked as a 'Merger' because they appear close together in the image, even when there are no other signs of interaction. Despite this, there is a clear enhancement of *Merger* features at $20 \lesssim r_p \lesssim 40\,h_{70}^{-1}$ kpc for $\Delta V < 500\,\mathrm{km\,s^{-1}}$ close pairs over that seen for the control sample. In the projection bias-corrected $F(r_p, Merger)$ we also see that physically interacting low-ΔV pairs do have an additional probability of being identified as a merger, although it is a noisy function of r_p.

The *Merger* answer displays crosstalk with the other 'Odd' categories. As $f(r_p, Merger)$ increases with decreasing r_p, the vote fractions of most of the alternative answers (i.e. *Ring*, *Arc*, *Disturbed*, *Irregular*, *Dust Lane*) decrease, for both the low-ΔV and control sample pairs. However, with the projection bias accounted for, at the smallest separations ($r_p < 10\,h_{70}^{-1}$ kpc), $F(r_p, Irregular)$ and $F(r_p, Disturbed)$ increase, possibly at the expense of $F(r_p, Merger)$. This is consistent with users preferentially classifying separated pairs as 'Mergers' and interpreting overlapping pairs as single 'Irregular' or 'Disturbed' objects. An enhancement of GZ2 *Dust Lane* features in merging early types has already been discussed by Shabala et al. (2012), although we only see a tentative indication of this with our method.

Interestingly, the *Other* category displays a contrasting behaviour, showing a decreasing $F(r_p, Other)$ with decreasing r_p. This appears

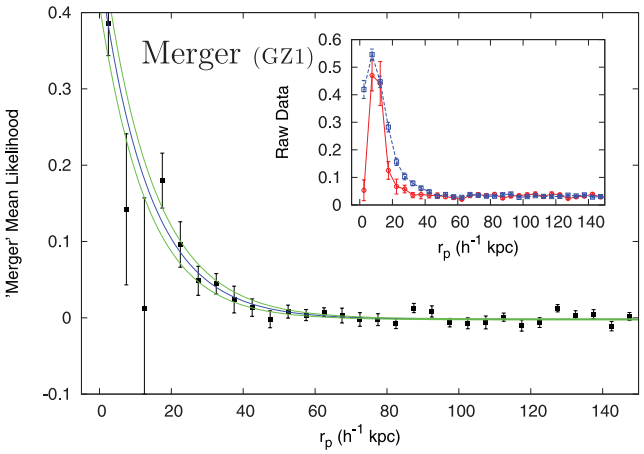

Figure 3. Mean vote fractions for the GZ1 *Merger* answer. The main plot shows the mean vote fraction of $\Delta V < 500\,\mathrm{km\,s^{-1}}$ close pairs, corrected for projection bias, i.e. $F(r_\mathrm{p}, A) = P(r_\mathrm{p}, A|\boldsymbol{M})$ (points with error bars), together with best fit (blue line) to these points using equation (8) and the corresponding 1σ confidence region (green lines). The insets plot $f(r_\mathrm{p}, A)$ for the $\Delta V < 500\,\mathrm{km\,s^{-1}}$ close pairs (blue) and $1000 < \Delta V < 5000\,\mathrm{km\,s^{-1}}$ control sample pairs (red), from which $F(r_\mathrm{p}, A)$ is calculated.

to be a result of other, more specific, categories being favoured for pairs with a real physical association. Looking at the *Other* button image in Fig. 1 it is clear why some projected close pairs are given this classification, especially non-interacting early-type galaxies.

All these results have important implications for the use of the GZ2 'Odd' classifications. In particular, they imply that for physically interacting close pairs, the likelihood of being classified as a merger actually begins to decreases at the smallest separations as galaxies begin to be classified more as irregular or disturbed. Given the large amount of projection bias and the crosstalk between categories, it is difficult to use any of the 'Odd' categories alone as indicators of pair interactions. It seems that using the more general *Odd=Yes* provides the most straightforward signal of interacting pairs.

For comparison, the GZ1 *Merger* class is plotted in Fig. 3. Since GZ2 uses a subset of the GZ1 sample, GZ1 classifications are available for all of the galaxies in our sample and the same galaxies are included in Figs 2 and 3. The GZ1 and GZ2 *Merger* classifications display the same behaviour with decreasing projected separation, with both showing a dip at the smallest separations ($r_\mathrm{p} < 10\,h_{70}^{-1}$ kpc). For GZ2 many of these *Merger* votes are exchanged for the *Irregular* and *Disturbed* categories, whereas for GZ1 it appears that the votes go to *Spiral-CW* and *Spiral-ACW* classifications, perhaps due to the formation of tidal arms. It is possible that similar effects have been present, but gone unnoticed, in previous work using more traditional classification schemes. Despite the presence of a significant signal for the control sample, in most separation bins the low-ΔV pairs display higher *Merger* vote fractions than high-ΔV pairs, and hence a sensible correction for this projection bias may be applied.

The parameters of the fitting functions, quantifying the amplitude and scale of the trends shown in Figs 2 and 3, are provided in Table 1.

4.2 Spiral arms and tidal tails

Although the 'Odd' GZ2 questions were targeted directly at identifying interactions, there are other morphological indicators available. Tidal interactions frequently induce or enhance spiral arm and tidal tail features. Indeed, we find that a number of the GZ2 answers regarding spiral features display a clear dependence on pair separation.

Table 1. Best-fitting results to the plots of $F(r_\mathrm{p}, A)$ in Figs 2–5 using equation (8). *Edge-on=No* and *Bar=No* are fits to trends with $20\,h_{70}^{-1}$ kpc bins; *Spiral*, *Loose Winding Arms*, *1 Arm*, *2 Arms* and *Other* use $10\,h_{70}^{-1}$ kpc bins, while *Odd*, *Merger*, *Irregular*, *Disturbed* and *Features* use $5\,h_{70}^{-1}$ kpc bins.

Answer	a	b (h_{70}^{-1} kpc)	c
Odd=Yes	0.54 ± 0.15	21 ± 3	-0.015 ± 0.002
Irregular	0.18 ± 0.05	8 ± 2	-0.016 ± 0.002
Disturbed	0.10 ± 0.02	6 ± 2	0.005 ± 0.002
Other	-0.23 ± 0.19	10 ± 9	-0.005 ± 0.003
Merger	0.31 ± 0.10	21 ± 4	-0.004 ± 0.002
GZ1 Merger	0.46 ± 0.05	14 ± 1	-0.002 ± 0.001
Features	0.22 ± 0.04	56 ± 13	-0.033 ± 0.006
Edge-on=No	0.55 ± 0.13	39 ± 11	0.005 ± 0.014
Bar=No	0.46 ± 0.20	28 ± 12	0.013 ± 0.012
Spiral=Yes	0.21 ± 0.04	66 ± 16	-0.036 ± 0.008
Loose Winding Arms	0.24 ± 0.03	33 ± 5	-0.006 ± 0.003
1 Arm	0.13 ± 0.02	23 ± 4	-0.001 ± 0.001
2 Arms	0.14 ± 0.04	79 ± 32	-0.014 ± 0.009

Fig. 4 presents the trends in 'Spiral' GZ2 morphological features as a function of pair separation. As shown in Fig. 2, the main panels plot the mean vote fraction, $F(r_\mathrm{p}, A)$, of $\Delta V < 500\,\mathrm{km\,s^{-1}}$ close pairs, after correcting for projection bias effects using the $1000 < \Delta V < 5000\,\mathrm{km\,s^{-1}}$ control sample (see Section 3.2). This quantity represents the probability, $P(r_\mathrm{p}, A|\boldsymbol{M})$, of a galaxy in this sample displaying the specified morphological attribute, purely as a result of being in a pair with separation r_p, provided it is meaningful to ask about that feature. The raw vote fractions, $f(r_\mathrm{p}, A)$, from which the corrected quantities are determined, are also shown in the inset panels. Although we still see some trends with r_p in the control sample, the projection biases are much less severe than those for the 'Odd' features considered above.

We first consider the probability that galaxies will be classified as displaying spiral features, given that they display any features and are not edge-on discs, $F(r_\mathrm{p}, \mathit{Spiral} = \mathit{Yes}) = P(r_\mathrm{p}, \mathit{Spiral} = \mathit{Yes}\,|\,\mathit{Features} \cap \mathit{Edge\text{-}on} = \mathit{No})$. We find that this increases significantly with decreasing projected separation, beginning around $r_\mathrm{p} \lesssim 100\,h_{70}^{-1}$ kpc. We see that the trends in $F(\mathit{Spiral} = \mathit{Yes})$ and $F(\mathit{2\,Arms})$ are similar, indicating that the increase in the probability of close pairs presenting spiral features is accompanied by an enhancement in the probability of those spiral features being two-armed. This increase in the probability of *2 Arms* is at the expense of the probability that the number of arms cannot be discerned. Together, these indicate a general strengthening of two-arm spiral patterns in close pairs on an exponential scale of $\sim 70\,h_{70}^{-1}$ kpc. This is consistent with observations and simulations which see an enhancement in spiral arm strength in interacting systems, often accompanied by an increase in star formation activity (e.g. Sundelius et al. 1987).

We can also consider the occurrence of different numbers of spiral arms. At small separations ($r_\mathrm{p} \lesssim 20\,h_{70}^{-1}$ kpc), the probability of a galaxy in a low-ΔV pair displaying a single spiral arm, $F(\mathit{1\,Arm})$, increases sharply. There is perhaps a suggestion that $F(r_\mathrm{p}, \mathit{2\,Arms})$ decreases somewhat as *1 Arm* increases at small r_p. The other answers to the 'How many spiral arms are there?' question show no significant change with decreasing pair separation.

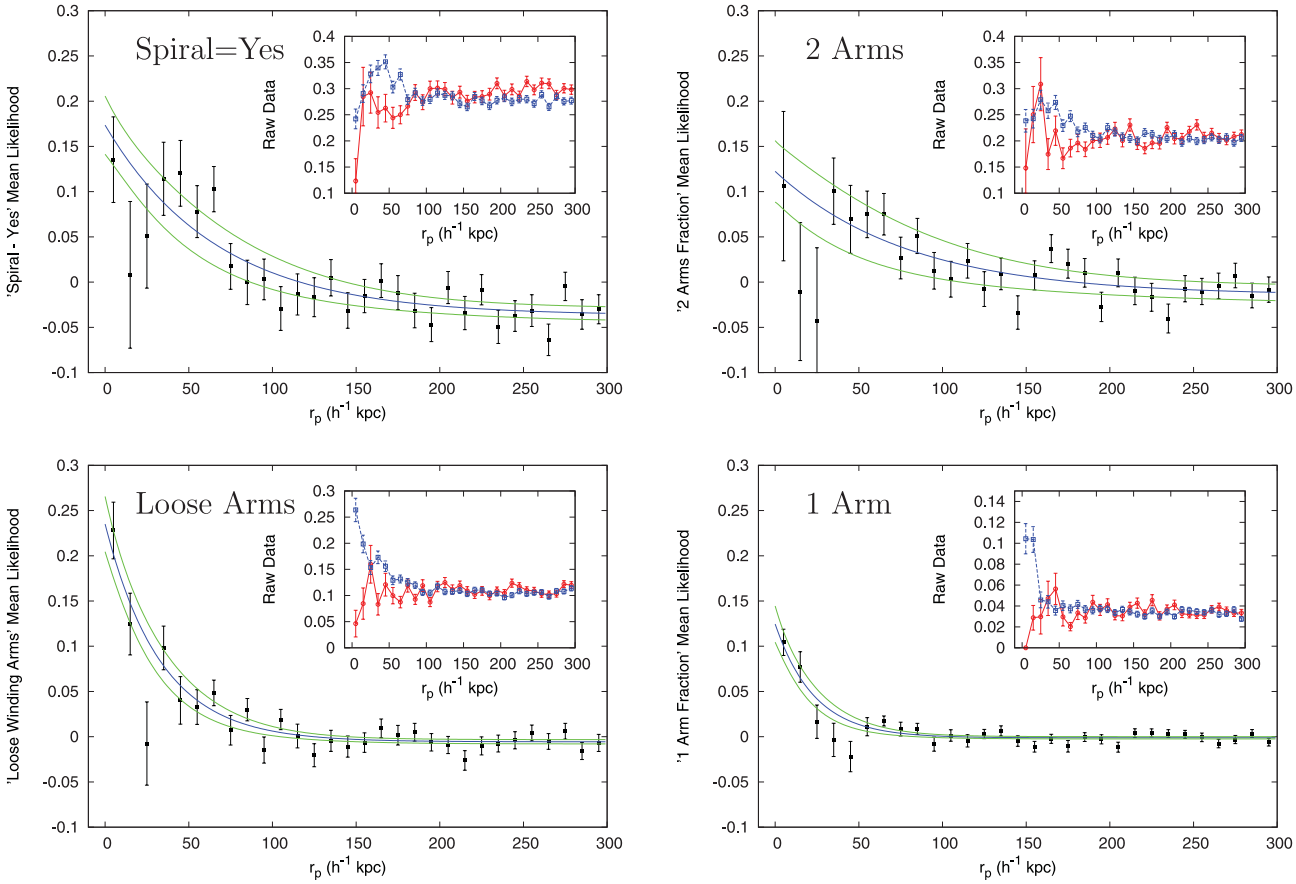

Figure 4. Mean vote fractions for the *Spiral=Yes* answer and answers to the subsequent 'arm number' and 'arm tightness' questions which show trends versus r_p: *1 Arm*, *2 Arms* and *Loose Winding Arms*. The main plot in each panel shows the mean vote fraction of $\Delta V < 500\,\mathrm{km\,s^{-1}}$ close pairs, corrected for projection bias, i.e. $F(r_p, A) = P(r_p, A|\boldsymbol{M})$ (points with error bars), together with best fit (blue line) to these points using equation (8) and the corresponding 1σ confidence region (green lines). The insets plot $f(r_p, A)$ for the $\Delta V < 500\,\mathrm{km\,s^{-1}}$ close pairs (blue) and $1000 < \Delta V < 5000\,\mathrm{km\,s^{-1}}$ control sample pairs (red), from which $F(r_p, A)$ is calculated.

Finally, we examine how the winding tightness of any spiral pattern depends on pair separation. In Fig. 4, we see that the probability of a galaxy being classified as having *Loose Winding Arms* (hereafter *LWA*) increases for $r_p < 100\,h_{70}^{-1}$ kpc. On the other hand, the *Medium Winding Arms* and *Tight Winding Arms* classes show no significant change with r_p. Although it has been known for some time that strong tidal interactions between galaxies can produce either one or two loosely wound tidal arms, depending on the orbital parameters (e.g. Thomasson et al. 1989; Howard et al. 1993; Barnes & Hibbard 2009; Barnes 2011), this is the first study to determine the observability of these features as a function of separation.

The *1 Arm* and *LWA* features appear to be particularly robust indicators of pair interaction, as the control samples display opposing behaviour to the physically associated pairs. In the absence of a true interaction, galaxies in projected pairs are actually less likely to be classified as having *1 Arm* or *LWA*. Given the limited impact of projection bias effects for these quantities, we could in principle use the low-ΔV pair trends in arm winding and arm number directly, without the need for remove the r_p dependence of the control sample. However, performing this correction gives us a more reliable and quantitative measurement of the trends. A price of this correction is noise added due to the limited size of the control sample.

It was originally envisaged that these questions would primarily provide information regarding the usual spiral arms, but it seems clear that in the case of close pairs they are revealing additional information. Observations and simulations of strong tidal galaxy interactions frequently show extended, asymmetric tails (see the discussion and references in Section 1). We therefore interpret the trends in $F(r_p, 1\,Arm)$ and $F(r_p, LWA)$ as unambiguous signatures of tidal tails caused by interactions between close pairs.

We also see an increase in the *Features* and *Edge-on=No* answers with decreasing pair separation. The increase in *Features* appears to be a result of galaxies that would have otherwise appeared smooth and featureless gaining enhanced spiral arms or tidal features in close pairs. Similarly, spiral galaxies which are being tidally disturbed may develop warped discs, and therefore be less likely to be classified as *Edge-on=Yes*. This could have the additional effect of preserving the visibility of the spiral arms, despite the high inclination. Moreover, at least in some cases, it appears that participants may interpret a warped edge-on disc as *LWA*.

The amplitude and scale of the trends shown in Fig. 4, in terms of the parameters of the best fit of equation (8), are provided in Table 1, along with the corresponding values for *Features* and *Edge-on=No*.

4.3 Barred galaxies

The identification and properties of barred galaxies in Galaxy Zoo are studied in detail by Masters et al. (2011, 2012) and Hoyle et al. (2011). The dependence of GZ2 bars on environment is presented in

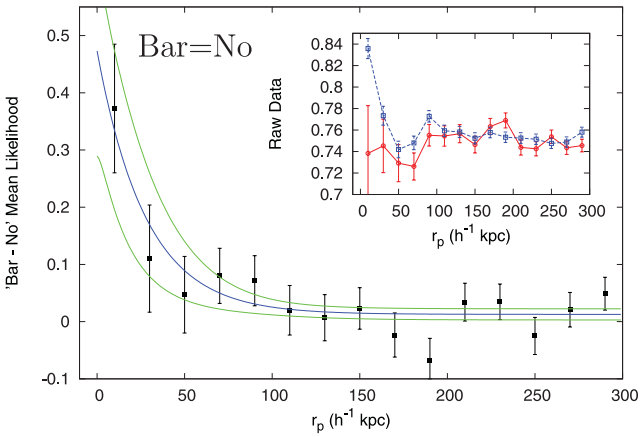

Figure 5. Mean vote fractions for the *Bar=No* answer. The main plot shows the mean vote fraction of $\Delta V < 500\,\mathrm{km\,s^{-1}}$ close pairs, corrected for projection bias, i.e. $F(r_\mathrm{p}, A) = P(r_\mathrm{p}, A|\boldsymbol{M})$ (points with error bars), together with best fit (blue line) to these points using equation (8) and the corresponding 1σ confidence region (green lines). The insets plot $f(r_\mathrm{p}, A)$ for the $\Delta V < 500\,\mathrm{km\,s^{-1}}$ close pairs (blue) and $1000 < \Delta V < 5000\,\mathrm{km\,s^{-1}}$ control sample pairs (red), from which $F(r_\mathrm{p}, A)$ is calculated.

Skibba et al. (2012). Here we continue our focus on the relationship between morphology and close pair interactions.

In Fig. 5, the corrected mean vote fraction for the *Bar=No* answer, $F(r_\mathrm{p}, Bar = No)$, is plotted versus projected separation. This trend was found to be rather noisy so we use $20\,h_{70}^{-1}$ kpc r_p bins to more clearly represent the data. There appears to be an increase in $F(r_\mathrm{p}, Bar = No)$ for $r_\mathrm{p} < 20\,h_{70}^{-1}$ kpc in the low-ΔV pairs, while the high-ΔV control sample pairs show no significant change with projected separation.

This result indicates that bars are suppressed, rather than triggered, by strong tidal interactions. It is possible that part of the observed trend is a result of bars becoming less noticeable in interacting pairs due to increased star formation and looser spiral arms, but even so there cannot be a strong enhancement of bars in our interacting pairs. This is in agreement with the preliminary findings of Méndez-Hernández et al. (2011) who compared isolated and paired galaxies and found the bar fraction to be ∼43 per cent for isolated galaxies, but only ∼20 per cent for pairs (where bars are identified in ellipse fits to the isophotes). Similarly, Lee et al. (2012) find that the fraction of visually classified strong bars decreases at small pair separations.

At first this seems contrary to the expectation that bar features are excited by gravitational interactions, as indicated by many simulation studies (e.g. Noguchi 1988; Moore et al. 1996; Moore, Lake & Katz 1998; Romano-Díaz et al. 2008), although in simulations including gas, tidal interactions appear less able to generate bars (e.g. Berentzen et al. 2004). There have also been observational indications of bar enhancement in dense environments and interacting systems (e.g. Elmegreen, Elmegreen & Bellin 1990). However, disc galaxies in denser environments are more massive and possess redder colours and earlier morphologies, all of which also correlate with the presence of bars (Masters et al. 2011). In a detailed study of this issue, Skibba et al. (2012) found a substantial enhancement in the appearance of bars in denser environments, but concluded that the majority of the effect was attributable to the dependence of colour and stellar mass on environment. However, a significant correlation remains, which Skibba et al. argue indicates that minor mergers and tidal interactions increase the appearance of bars by triggering disc instabilities. They also find the bar–environment correlation to decrease at small separations, becoming statistically insignificant at $r_\mathrm{p} < 150\,h_{70}^{-1}$ kpc. While not identical to our close pair results, this is nevertheless consistent. Simulations also demonstrate the suppression or destruction of bars in strong tidal interactions (Berentzen et al. 2003). However, most simulation work focuses on the final result of pair interactions, rather than the evolution of morphological features over the course of the interaction. In the low-mass ratio pairs we study in this paper, the final result of the interaction may often be the destruction of any bars along with their entire disc. Theoretically, it seems that destruction of bars at earlier stages of pair interactions is feasible, and the observations, in this paper and by others, appear to indicate this. The emerging picture is therefore that moderate interactions, with high-mass ratios (i.e. minor mergers and harassment), promote bar formation, but that stronger interactions suppress the appearance of bars.

4.4 Dependence of tidal effects on line-of-sight velocity difference

So far we have been considering the r_p dependence for a fixed sample of pairs with $\Delta V < 500\,\mathrm{km\,s^{-1}}$, versus a control sample with $1000 < \Delta V < 5000\,\mathrm{km\,s^{-1}}$. However, we would also expect a relationship between physical separation, and hence interaction strength, and ΔV. This is explored in Fig. 6, in which we plot $F(r_\mathrm{p}, LWA)$ for pairs in several bins of ΔV. Again, we fit the data with equation (8) in an attempt to quantify the trends. Due to the limited statistics, these plots are relatively noisy and the fit parameters are sometimes quite uncertain. Nevertheless, some trends are clearly seen in both the raw data and the fits.

Signs of interaction appear strong for the smallest ΔV pairs, and weaken with increasing ΔV. We see almost no signs of interaction for $\Delta V > 500\,\mathrm{km\,s^{-1}}$. In Table 2, we see that for $\Delta V > 300\,\mathrm{km\,s^{-1}}$ the fitting parameter a (representing the excess *LWA* likelihood at $r_\mathrm{p} = 0\,h_{70}^{-1}$ kpc) decreases sharply. As ΔV decreases, there is a hint that pairs show signs of tidal interactions further out. This would be consistent with our expectations: pairs with low ΔV must be predominantly interacting in the plane of the sky, whereas at higher ΔV, pairs will be increasingly interacting along the line of sight.

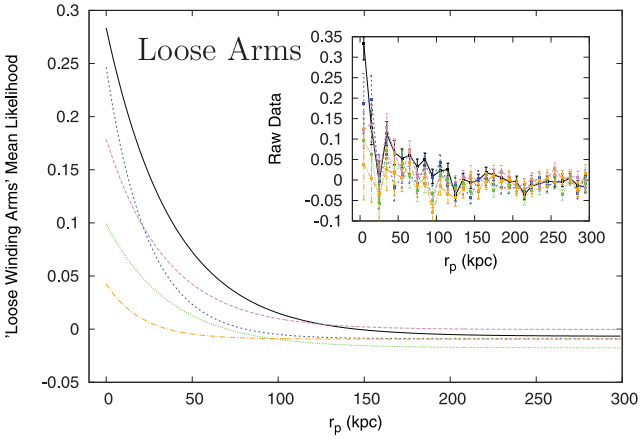

Figure 6. The trend in the probability of observing *Loose Winding Arms* with projected separation, $F(r_\mathrm{p}, LWA)$, for pair samples selected with different ranges in ΔV: $0 < \Delta V < 100\,\mathrm{km\,s^{-1}}$ (black), $100 < \Delta V < 200\,\mathrm{km\,s^{-1}}$ (purple), $200 < \Delta V < 300\,\mathrm{km\,s^{-1}}$ (blue), $300 < \Delta V < 400\,\mathrm{km\,s^{-1}}$ (green) and $400 < \Delta V < 500\,\mathrm{km\,s^{-1}}$ (yellow). The low-ΔV pairs clearly show stronger signs of interaction than the high-ΔV pairs.

Table 2. Best-fitting results to the plots of $F(r_p, LWA)$ in Fig. 6 for a range of ΔV bins using equation (8). The fits are done using $10\,h_{70}^{-1}$ kpc bins.

ΔV (km s^{-1})	a	b (h_{70}^{-1} kpc)	c
$0 < \Delta V < 100$	0.29 ± 0.04	39 ± 5	-0.007 ± 0.003
$100 < \Delta V < 200$	0.18 ± 0.04	35 ± 9	-0.000 ± 0.004
$200 < \Delta V < 300$	0.26 ± 0.08	24 ± 7	-0.009 ± 0.004
$300 < \Delta V < 400$	0.12 ± 0.05	37 ± 18	-0.018 ± 0.005
$400 < \Delta V < 500$	0.05 ± 0.11	21 ± 44	-0.009 ± 0.004

In future work we intend to treat ΔV and r_p on similar terms, quantifying the dependence of observed morphological features as a function of both quantities.

4.5 Identifying probable interacting galaxies

As we have seen above, the strongest indication of interacting galaxies in physically associated pairs is an enhanced probability of being classified with *Loose Winding Arms*. Previously we have studied this signal statistically, averaged over many galaxies in bins of r_p. We now attempt to use this morphological signature to identify galaxies which are likely to be interacting, by selecting those which have $f(LWA)$ above a certain threshold. After visually examining ∼100 galaxies with a range of thresholds we found that $f(LWA) > 0.6$ is sufficient to reliably identify galaxies with tidal features, provided there are at least two *LWA* votes. (A single vote may occasionally be spurious.) Given the roughly similar number of times each object has been classified, the requirement of at least two *LWA* votes may be expressed as a threshold on $p(\boldsymbol{M})$. In this case, $p(\boldsymbol{M}) = p(Features \cap Edge\text{-}on = No \cap Spiral = Yes) = f(Features)\,f(Edge\text{-}on = No)\,f(Spiral = Yes)$, which we hereafter refer to as $p(FNS)$. Most GZ2 objects have at least 30 classifications, so applying a threshold of $p(FNS) > 0.1$ means that the question 'How tight are the spiral arms?' has received at least three answers, at least two of which must have indicated *Loose Winding Arms* if $f(LWA) > 0.6$. As described in Section 3.2, we denote this selection as $f(LWA \mid p(FNS) > 0.1) > 0.6$.

The chosen thresholds are a reasonable compromise. If we choose lower thresholds we select potential interacting galaxies with more subtle tidal features, but at the same time increase the contamination from non-interacting pairs. The number of galaxies which satisfy our criteria will inevitably represent only a fraction of the galaxies which are truly interacting. Some galaxies may possess tidal features that are unobservable [i.e. do not result in a significantly elevated $f(LWA)$] due to their low surface brightness, an unfavourable sky orientation (i.e. edge-on galaxies) or other observational limitation. Other truly interacting galaxies may possess only weak, or entirely absent, morphological signatures of that interaction, due to the orbital parameters of the interaction. As discussed by Toomre & Toomre (1972), galaxies which are rotating in the same sense as the orbital pass of the companion will form tidal arms which are much more pronounced than if the galaxy is rotating in the opposite direction. Finally, galaxies which display *Loose Winding Arms* have probably already undergone at least one close pass of their companion. Some close pairs will be in the early stages of their interaction and thus have not yet formed tidal arms.

We visually examined all of the galaxies in pairs with $r_p < 200\,h_{70}^{-1}$ kpc and $\Delta V < 500\,\mathrm{km\,s^{-1}}$ and selected to be interacting with $f(LWA \mid p(FNS) > 0.1) > 0.6$. Essentially all of these objects show obvious signs that they are interacting with a companion. In many cases the companion is also selected as interacting. However, galaxies can belong to multiple pairs and most of the interacting galaxies in large separation ($r_p \gtrsim 100\,h_{70}^{-1}$ kpc) pairs were actually found to have a closer companion that is likely to be the true cause of the interaction. In these cases the companion at larger separation typically shows no signs of interaction, and may not be physically associated. This is also the case for some very close pairs, where the closest companion is actually an interloper, and the interacting companion is at a larger projected separation. Moreover, due to the redshift incompleteness of the SDSS, especially at small angular separations, some of the interacting companions of galaxies identified as having *Loose Winding Arms* will be missing from our sample.

Table 3 shows examples of galaxies with *Loose Winding Arms*, i.e. $f(LWA \mid p(FNS) > 0.1) > 0.6$, for a range of r_p up to $100\,h_{70}^{-1}$ kpc. We see that the high-mass pairs consist mostly of early-type galaxies, while the lower mass pairs are mostly mixed- and late-type pairs with bluer colours.

4.6 Accounting for interlopers in the frequency of galaxy pair interactions

In this section, we demonstrate how morphological indicators of interaction may be used to refine estimates of the frequency of galaxy pair interactions. We employ a mass-limited sample, selected by imposing a minimum mass limit of $10^{9.5}\,\mathrm{M}_\odot$ and redshift limits of $0.01 < z < 0.05$, giving a sample of 44 064 galaxies. The highest mass galaxies in our sample have $M_* \sim 10^{11.5}\,\mathrm{M}_\odot$. We consider all galaxy pairs with $\Delta V < 500\,\mathrm{km\,s^{-1}}$ and $r_p < 300\,h_{70}^{-1}$ kpc, in $5\,h_{70}^{-1}$ kpc bins.

As we have seen, a significant fraction of the galaxies in these pairs will not be truly interacting. Previous studies have found this contamination to a strong function of projected separation (Alonso et al. 2004; Perez et al. 2006) and galaxy luminosity (and thus mass), with the faintest pairs being most affected (Patton & Atfield 2008). We therefore use the morphological indicators of interactions, explored above, to estimate and correct for the influence of interlopers on our determination of the interaction rate.

We calculate the average number of companions at separation r_p (and within $\Delta V < 500\,\mathrm{km\,s^{-1}}$) for each galaxy in the sample, $N_c(r_p)$, following the method in Section 3.3 (with $w_{int} = 1$). This method accounts for the various sample selection issues to produce a corrected estimate of the average number of close companions per galaxy. As some of these companions will not be physically interacting, this is an upper limit on the number of interacting companions per galaxy.

We also measure the average number of companions in pairs displaying *Loose Winding Arms*, $N_{cLWA}(r_p)$. This is achieved in an identical fashion, but limited to probable interacting galaxies where at least one member of a pair is identified as having *Loose Winding Arms*, using the criteria developed in Section 4.5, i.e. $w_{int} = 1$ if $f(LWA \mid p(FNS) > 0.1) > 0.6$ for either member of the pair and $w_{int} = 0$ otherwise.

The fraction of companion galaxies which show indications of possible interaction (i.e. with $f(LWA \mid p(FNS) > 0.1) > 0.6$) can be calculated for each r_p bin using

$$\mathcal{F}_{LWA}(r_p) = \frac{N_{cLWA}(r_p)}{N_c(r_p)}\,. \tag{12}$$

Table 3. Galaxies selected to be interacting members of a pair, using $f(LWA \mid p(FNS) > 0.1) > 0.6$ and $\Delta V < 500\,\mathrm{km\,s^{-1}}$. The figures along the top indicate the approximate r_p (in h_{70}^{-1} kpc) of the pairs in each column. The other figures give the stellar masses (in $\mathrm{M}_\odot$) of galaxies in the adjacent image. The top and bottom rows present examples with high and low stellar masses, respectively. The width of these figures is $\sim 110\,h_{70}^{-1}$ kpc, based on the average redshift of the pair.

r_p (h_{70}^{-1} kpc)	5	15	25	35	45	55	65	75	85	95
M_* ($M_\odot$)	11.0–10.4	10.9–10.8	10.9–11.1	10.7–11.0	10.7–11.1	10.8–10.9	11.0–11.2	11.0–11.1	10.8–11.1	10.9–11.2
	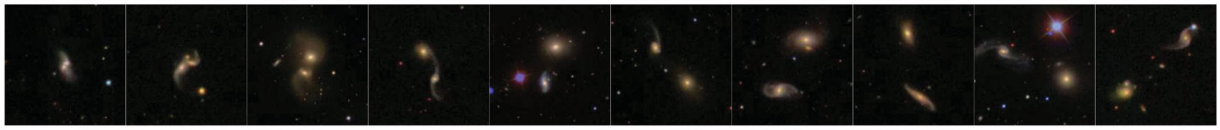									
M_* ($M_\odot$)	9.9–10.1	9.5–9.5	10.0–10.4	10.0–10.3	10.0–10.1	9.8–9.6	9.6–9.9	9.8–10.1	9.7–9.8	9.8–10.2
										

This fraction is related to the true interacting fraction, $\mathcal{F}_\mathrm{int}(r_\mathrm{p})$, such that

$$\mathcal{F}_\mathrm{int}(r_\mathrm{p}) = \frac{\mathcal{F}_{LWA}(r_\mathrm{p}) - \mathcal{F}_{LWA}(r_\mathrm{p} \to \infty)}{P_\mathrm{intobs}}\,, \tag{13}$$

where $\mathcal{F}_{LWA}(r_\mathrm{p} \to \infty)$ gives the fraction of galaxies passing our *LWA* selection in the absence of pair interactions probed by our sample selection. These galaxies are mostly interlopers, associated in projection with truly interacting pairs: a galaxy with *LWA* interacting with one physically close companion could also have additional, non-interacting, companions at any r_p. These companions would be (falsely) counted as interacting in equation (12). Some galaxies may also display *LWA* features due to intrinsic properties of the galaxies or due to interactions with companions possessing masses lower than our sample selection. Both these cases are accounted for by subtracting $\mathcal{F}_{LWA}(r_\mathrm{p} \to \infty)$ in equation (13).

The factor P_intobs converts the fraction of galaxies in pairs displaying *LWA* into the fraction of truly interacting galaxies. It is the average probability of a true physical interaction resulting in an observable *LWA* signature in our data set. In principle, P_intobs could be a function of r_p, although we expect it to vary slowly. Remember that our working definition of an 'interaction', from Section 1, is that a galaxy has experienced a significant tidal force, compared to its gravitational binding force, averaged over the previous dynamical time. For a given data set, the level of tidal force that is deemed 'significant' is that which results in observable features in the most favourable circumstances. Variations of P_intobs from a constant with r_p are therefore only expected from secondary effects. However, this assumption would greatly benefit from being tested with simulations, which would potentially result in a refined functional form for P_intobs. For the time being, we assume a constant P_intobs. Although the *LWA* class is a rather indirect indicator of tidal tails, P_intobs accounts for the difference between the number of objects actually counted and the number missed. Future refinements to P_intobs could include a more careful consideration of the conditions under which interactions produce tidal tails that would be classified as loose spirals.

Fig. 7 plots $\mathcal{F}_{LWA}(r_\mathrm{p})$ and a fit to the trend using equation (8). The best fit gives parameter values $a_{\mathcal{F}_{LWA}} = 0.236$, $b_{\mathcal{F}_{LWA}} = 20.145\,h_{70}^{-1}$ kpc and $c_{\mathcal{F}_{LWA}} = 0.035$. At large r_p the curve levels off to a constant value, $\mathcal{F}_{LWA}(r_\mathrm{p} \to \infty) = c_{\mathcal{F}_{LWA}}$. Therefore,

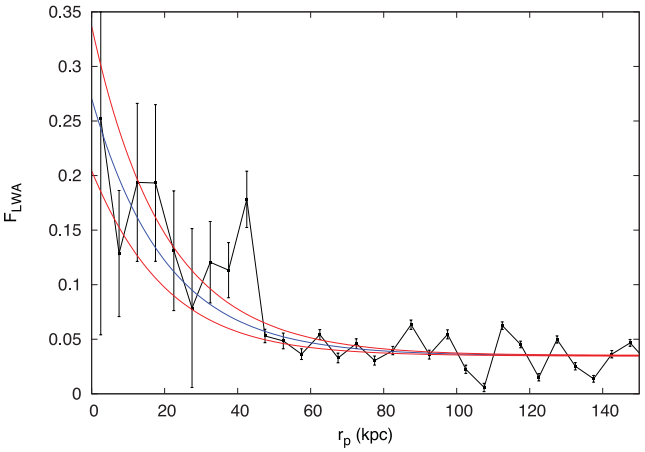

Figure 7. Pairs containing at least one member with $f(LWA \mid p(FNS) > 0.1) > 0.6$ divided by the total number of pairs in each r_p bin. Results are given for $\Delta V < 500\,\mathrm{km\,s^{-1}}$ (black line), together with a fit using equation (8) (blue line) and the corresponding 1σ confidence region (red lines).

$$\mathcal{F}_\mathrm{int}(r_\mathrm{p}) = \frac{a_{\mathcal{F}_{LWA}} \exp(-r_\mathrm{p}/b_{\mathcal{F}_{LWA}})}{P_\mathrm{intobs}}\,. \tag{14}$$

We may place strong constraints on P_intobs by noticing that $\mathcal{F}_\mathrm{int}(r_\mathrm{p})$ must lie on the interval [0, 1]. Therefore, a constant P_intobs must lie on the interval $[a_{\mathcal{F}_{LWA}}, 1]$, and hence

$$\mathcal{F}_\mathrm{int}(r_\mathrm{p}) = [a_{\mathcal{F}_{LWA}}, 1] \times \exp(-r_\mathrm{p}/b_{\mathcal{F}_{LWA}})\,, \tag{15}$$

where the square brackets denote an interval. This provides the means to calculate strong limits on the true frequency of interactions from our observations of galaxies with *LWA* features.

We can determine an estimate of the average number of interacting companions for galaxies in our sample, $N_{\mathrm{c\,int}}(r_\mathrm{p})$, by applying an r_p-dependent weight, w_int, in the methodology of Section 3.3. This weight is simply the fraction of companions at r_p that are truly

interacting galaxies, so $w_{\rm int} = \mathcal{F}_{\rm int}(r_{\rm p})$. For our sample, using the parameters of the fit to $\mathcal{F}_{LWA}(r_{\rm p})$ in Fig. 7, we derive the interval

$$w_{\rm int} = [0.236, 1.0] \times \exp(-r_{\rm p}/20.145\, h_{70}^{-1}\,{\rm kpc})\,. \quad (16)$$

Usually when one calculates the close companion frequency, one must apply an $r_{\rm p}$ limit. Using $w_{\rm int}$, however, weights companions by the likelihood that pairs with that projected separation are truly interacting. One can therefore integrate to large $r_{\rm p}$ and determine a total frequency of interacting companions. To illustrate, without the interaction weighting (i.e. $w_{\rm int} = 1$ in equation 9), considering pairs with small projected separations gives $N_{\rm c}(r_{\rm p} < 30\, h_{70}^{-1}\,{\rm kpc}) = 0.028 \pm 0.002$. Including the $w_{\rm int}$ given by equation (16) results in $N_{\rm cint}(r_{\rm p} < 30\, h_{70}^{-1}\,{\rm kpc}) = [0.0033 \pm 0.0010, 0.014 \pm 0.004]$, where the interval brackets the allowed range of probabilities, $P_{\rm intobs}$, that an interaction results in an observable *LWA* feature. Comparing $N_{\rm c}$ and the upper limit for $N_{\rm cint}$ implies that at least 49 ± 14 per cent of pairs with $r_{\rm p} < 30\, h_{70}^{-1}$ kpc, $\Delta V < 500\,{\rm km\,s^{-1}}$ and $M_* > 10^{9.5}\,{\rm M}_\odot$, are non-interacting interlopers. This agrees with the results of Patton et al. (2000), which found using visual classifications that ∼50 per cent of galaxies were interlopers for a similar range of $r_{\rm p}$, ΔV and M_*.

If we select all pairs up to our limiting projected separation, we find that $N_{\rm c}(r_{\rm p} < 300\, h_{70}^{-1}\,{\rm kpc}) = 0.62 \pm 0.004$, i.e. most galaxies have a companion within this distance. On the other hand, the average number of physically interacting companions per galaxy is $N_{\rm cint}(r_{\rm p} < 300\, h_{70}^{-1}\,{\rm kpc}) = [0.0048 \pm 0.0014, 0.021 \pm 0.006]$. This implies that >96 per cent of pairs with $r_{\rm p} < 300\, h_{70}^{-1}$ kpc, $\Delta V < 500\,{\rm km\,s^{-1}}$ and $M_* > 10^{9.5}\,{\rm M}_\odot$ are not actually interacting. Our method enables one to estimate the fraction of interacting galaxies without requiring an arbitrary cut-off in projected separation, and without any need for further contamination corrections.

Note that while we have developed a more sophisticated treatment of $r_{\rm p}$ trends here, we are still using a simple cut in ΔV. In principle, the method outlined here could possibly be extended to determine an interaction weight, $w_{\rm int}$, with dependence on both $r_{\rm p}$ and ΔV. There is also the potential of further constraining the interaction frequency by combining multiple indicators of interaction, rather than *LWA* alone. This approach could perhaps also enable the identification of pairs at different stages in their interaction, or with specific orbital characteristics. We leave all of these challenges for future work. A paper using the methods outlined above, to explore the dependence of the interaction frequency on stellar mass and environment, is in preparation.

5 SUMMARY AND DISCUSSION

In this paper, we have examined a variety of morphological signatures of interaction between galaxy pairs and demonstrated how the trends in these observable features, as a function of projected separation, can provide a refined estimate of the frequency of pair interactions in the galaxy population. We consider an 'interacting' galaxy to be one which has experienced a significant tidal force, compared to its gravitational binding force, averaged over the previous dynamical time (see Section 1). The tidal force deemed 'significant' depends upon the properties of a given observational data set.

We began by presenting our sample and the methods we employ, and particularly, in Section 3.2, discussing the information provided by Galaxy Zoo 2 and its interpretation in terms of the probability that a given galaxy is observed to possess a particular set of morphological features. We also presented a method to correct for 'projection bias', an effect whereby the signal of certain morphological features may depend on the apparent separation of galaxy pairs, even in the absence of any possible physical associations between pair members.

In Section 4.1 we considered questions from GZ2 designed to identify *Odd* features, including answers, such as *Merger*, which were intended to identify signs of interaction. We found that these classifications suffer from a strong projection bias. For example, galaxies with small projected separation, but very large velocity offsets, tend to have a spuriously large *Merger* signal. Furthermore, the way in which the question for these *Odd* features was arranged, allowing only one of the available options to be selected, results in crosstalk between the *Odd* categories, in terms of both true signal and projection bias, which complicates their interpretation. We find that this projection bias is also present for the GZ1 *Merger* classification, and shows a behaviour very similar to its GZ2 equivalent. Previous studies which used the GZ1 *Merger* class to identify merger candidates (Darg et al. 2010a,b) will have suffered to some degree from this issue, but the effect is probably relatively small due to their use of vote fraction thresholds and the fact that the low-ΔV galaxy pairs have a larger mean *Merger* vote fraction at most projected separations relative to the control sample pairs. In future iterations of Galaxy Zoo, and other visual classification efforts, it would be preferable to keep questions regarding different types of features distinct, or allow multiple answers to be selected for a single question when the relevant features are not mutually exclusive.

Nevertheless, the *Odd* classifications do provide useful information on the reality of galaxy interactions, particularly once a correction for the projection bias is applied by reference to a control sample of pairs with large velocity offsets. As discussed by Darg et al. (2010a) with relation to GZ1, the GZ2 *Merger* class (and also *Odd=Yes*) primarily selects interacting galaxies at small projected separations. It therefore mainly probes close passes and the later stages of mergers. We further find that the *Irregular* and *Disturbed* classes can identify interacting galaxies with very small projected separations, which may be either at an advanced stage of merging or aligned along the line of sight.

We have searched all the GZ2 classifications for trends with projected separation, and find significant signals with respect to the presence and form of spiral arms. The observability of spiral arms (*Spiral=Yes*), and particularly the dominant *2 Arms* class, is enhanced for close pairs on a scale of $r_{\rm p} \lesssim 70\, h_{70}^{-1}$ kpc. Darg et al. (2010a) find that the spiral-to-elliptical ratio for galaxies classified as mergers in GZ1 is approximately twice the global ratio, and in Darg et al. (2010b) conclude that this is due to the longer timescale over which spiral mergers are detectable compared to elliptical mergers. Our results show that this ratio can also be at least partly explained by the enhancement and formation of spiral arms in interacting galaxies. More unusual spiral arm features also present a trend with $r_{\rm p}$. The occurrence of *One Arm* spirals dramatically increases for small separations (on a scale of $r_{\rm p} \lesssim 20\, h_{70}^{-1}$ kpc), while *Loose Winding Arms* show the strongest increase (operating on an intermediate scale of $r_{\rm p} \lesssim 30\, h_{70}^{-1}$ kpc).

There are two principal ways in which spiral-like features can be created through tidal interactions. Tidal perturbations can instigate or amplify instabilities in gas discs, leading to the formation or enhancement of star formation in spiral arms similar to those seen in isolated galaxies (e.g. as seen by Xu et al. 2010). Tidal forces can also strip stars and gas out of the galaxies, forming tidal tails, counter tails and bridges, which may or may not harbour star formation (e.g. Mullan et al. 2011). We appear to detect both

signatures: an enhancement of 'normal' spiral arm features, occurring at large projected separations, with the signatures of stronger tidal interactions becoming increasingly prevalent at smaller separations. The tidal nature of the *Loose Winding Arms* features is confirmed by examination of typical images, such as those in Table 3. It is clear that many of the galaxies which have significant probability of *Loose Winding Arms*, especially those with higher stellar mass, are red, early-type galaxies. This indicates that the loose spiral features that are observed in these galaxies, and probably also those same features in star-forming, late-type galaxies, are the result of tidal stripping. In galaxies with sufficient cold gas, there will almost certainly be star formation in these tidal spiral features, and indeed in Table 3 we see that several of the galaxies possess very blue loose spiral arms. Simulations (e.g. Toomre & Toomre 1972; Howard et al. 1993; Barnes 2011) indicate that tidal features, such as those apparently identified by the GZ2 *Loose Winding Arms* class, are indicative of a stage between close passes, primarily between first and second pass, when pairs can still attain relatively large separations. The *Loose Winding Arms* features are thus probing the early stage of mergers and pair interactions.

The onset and appearance of tidal arms are known to depend on the geometry of the encounter. Numerical studies demonstrate that in-plane, prograde encounters produce the most symmetrical two-sided disturbances, while polar encounters give the most one-sided disturbances, and retrograde encounters are the last to make tidal tails (e.g. Thomasson et al. 1989; Howard et al. 1993; Barnes & Hibbard 2009; Barnes 2011). Retrograde encounters also produce the greatest increase in star formation efficiency (Cox et al. 2008). Considering this, the galaxies which are selected as having *2 Arms* and *Loose Winding Arms* in GZ2 are likely the result of prograde, in-plane encounters, while galaxies identified as displaying *1 Arm* are likely the result of polar or retrograde encounters. Our observed separation scales for these different features are consistent with this interpretation (see Table 1).

When comparing our results to other studies which look at the onset of tidally induced changes in interacting galaxies, we find that answers to Galaxy Zoo questions regarding spiral arms detect changes at separations similar to studies of tidally induced star formation, as discussed in Section 1. The *Loose Winding Arm* class begins to detect interacting galaxies around $r_{\rm p} \lesssim 120\,h_{70}^{-1}$ kpc, which is similar to the separation scale associated with induced star formation (Nikolic et al. 2004; Li et al. 2008; Patton et al. 2011). The star formation detected at these large separations is relatively weak, while a strong increase is observed for $r_{\rm p} \lesssim 40\,h_{70}^{-1}$ kpc (Ellison et al. 2008; Li et al. 2008; Robaina et al. 2009; Patton et al. 2011). This corresponds to scale for which we observe an enhancement of the *Merger* class. Quantitative morphological measurements also typically present signals on these scales (Hernández-Toledo et al. 2005; De Propris et al. 2007; Ellison et al. 2010). Logically, kinematic disturbance must precede morphological disturbance and so it might seem that star formation, if it is triggered by kinematical perturbations, should be an earlier indication of interaction than morphology (e.g. Byrd & Howard 1992). However, this paper shows that some morphological signatures are as sensitive as enhanced star formation, and more unambiguously related to interaction.

In Section 4.3, we found that the likelihood of a bar being observed decreases sharply for pairs with projected separations $r_{\rm p} \lesssim 20\,h_{70}^{-1}$ kpc. Bars are thought to be created through periodic orbital resonance (Bournaud & Combes 2002) and are known to initiate radial gas inflows, which in the end act to destroy or weaken the bar structure (Pfenniger & Norman 1990) [for a recent review see Sellwood & Sánchez (2010), or more comprehensively Sellwood & Wilkinson (1993)]. Gas inflows, perhaps together with the enhancement of bar features, caused by tidal perturbations in the early stages of major interactions may similarly act to rapidly destroy any pre-existing or transient bars (e.g. Berentzen et al. 2003; Di Matteo et al. 2007). Our results suggest that this is indeed the case, with the appearance of bars being strongly suppressed in close pairs, in agreement with other recent studies by Méndez-Hernández et al. (2011) and Lee et al. (2012). Eventually, the violent reorganization of stellar orbits in the later stages of many major interactions (i.e. mergers) must act to erase any orbital resonances which created the bar.

In Section 4.5, we focus on using the presence of *Loose Winding Arms* to identify probable interacting galaxies. These criteria are then used in Section 4.6 to constrain the frequency of galaxy pair interactions, without requiring an arbitrary cut-off in projected separation or any further corrections for contamination of our close pair sample. We find that the fraction of galaxies with $M_* > 10^{9.5}\,{\rm M}_\odot$ and $0.01 < z < 0.05$ that are in truly interacting pairs with $\Delta V < 500\,{\rm km\,s^{-1}}$ is in the range 0.5 ± 0.1 to 2.1 ± 0.6 per cent. The limits correspond to assuming the maximum and minimum permitted probability, $P_{\rm intobs}$, that interacting galaxies produce observable *Loose Winding Arms* features, respectively. We expect simple extensions of our technique to lead to significantly tighter confidence intervals in future work.

It is difficult to precisely compare our estimate of the interacting galaxy fraction to other studies, due to the range of different methods employed. Although the close pair fraction is mostly constant with luminosity (Patton & Atfield 2008), the limiting mass ratio and projected separation, varying definitions for selecting pairs, and many other subtleties, make comparisons complicated. Given that the estimate in this paper is derived from a relatively simple demonstration of combining close pair and morphological information, we defer such involved comparisons to future work. Nevertheless, we note that the major interaction fractions quoted by other recent studies, e.g. 1.1 ± 0.5, 2.1 ± 0.1, 1.6 ± 0.1 and 1.3 ± 0.1 by Bell et al. (2006), Patton & Atfield (2008), Domingue et al. (2009) and Xu et al. (2012), respectively, are neatly bracketed by our estimate of 0.4–2.7 per cent. This lends support for our use of GZ2 *Loose Winding Arms* as indicators of pair interactions, and encourages confidence in the method described in Section 4.6, and the various assumptions we have made.

ACKNOWLEDGMENTS

This publication has been made possible by the participation of more than 200 000 volunteers in the Galaxy Zoo project. Their contributions are individually acknowledged at http://authors.galaxyzoo.org.

Much of the work presented was performed while KRVC was hosted at the University of Nottingham, on a visit funded by a research travel grant from the Government of Catalunya, Spain (ref. 2010 BE-00268). KRVC would also like to thank Ben Hoyle for introducing him to Galaxy Zoo and getting him started on this project.

SPB gratefully acknowledges receipt of an STFC Advanced Fellowship.

KLM acknowledges funding from The Leverhulme Trust as a 2010 Early Career Fellow.

Support for the work of KS was provided by NASA through Einstein Postdoctoral Fellowship grant number PF9-00069 issued by the Chandra X-ray Observatory Center, which is operated by the

Smithsonian Astrophysical Observatory for and on behalf of NASA under contract NAS8-03060.

Finally, we thank the referee, Curt Struck, for his helpful comments and suggestions in preparing this work for publication.

REFERENCES

Adelman-McCarthy J. K. et al., 2008, ApJS, 175, 297
Alonso M. S., Tissera P. B., Coldwell G., Lambas D. G., 2004, MNRAS, 352, 1081
Arp H., 1966, ApJS, 14, 1
Bamford S. P. et al., 2009, MNRAS, 393, 1324
Barnes J. E., 2011, MNRAS, 413, 2860
Barnes J. E., Hernquist L., 1992, ARA&A, 30, 705
Barnes J. E., Hernquist L., 1996, ApJ, 471, 115
Barnes J. E., Hibbard J. E., 2009, AJ, 137, 3071
Bell E. F. et al., 2006, ApJ, 640, 241
Berentzen I., Athanassoula E., Heller C. H., Fricke K. J., 2003, MNRAS, 341, 343
Berentzen I., Athanassoula E., Heller C. H., Fricke K. J., 2004, MNRAS, 347, 220
Bournaud F., Combes F., 2002, A&A, 392, 83
Bridge C. R., Carlberg R. G., Sullivan M., 2010, ApJ, 709, 1067
Bushouse H. A., 1986, AJ, 91, 255
Bushouse H. A., 1987, ApJ, 320, 49
Byrd G. G., Howard S., 1992, AJ, 103, 1089
Charlton J. C., Salpeter E. E., 1991, ApJ, 375, 517
Conselice C. J., 2003, ApJS, 147, 1
Cox T. J., Jonsson P., Somerville R. S., Primack J. R., Dekel A., 2008, MNRAS, 384, 386
Darg D. W. et al., 2010a, MNRAS, 401, 1043
Darg D. W. et al., 2010b, MNRAS, 401, 1552
De Propris R., Conselice C. J., Liske J., Driver S. P., Patton D. R., Graham A. W., Allen P. D., 2007, ApJ, 666, 212
Di Matteo P., Combes F., Melchior A.-L., Semelin B., 2007, A&A, 468, 61
Domingue D. L., Xu C. K., Jarrett T. H., Cheng Y., 2009, ApJ, 695, 1559
Ellison S. L., Patton D. R., Simard L., McConnachie A. W., 2008, AJ, 135, 1877
Ellison S. L., Patton D. R., Simard L., McConnachie A. W., Baldry I. K., Mendel J. T., 2010, MNRAS, 407, 1514
Elmegreen D. M., Elmegreen B. G., Bellin A. D., 1990, ApJ, 364, 415
Fukugita M. et al., 2007, AJ, 134, 579
Gerber R. A., Lamb S. A., 1994, ApJ, 431, 604
Hernández-Toledo H. M., Avila-Reese V., Conselice C. J., Puerari I., 2005, AJ, 129, 682
Hopkins P. F., Cox T. J., Kereš D., Hernquist L., 2008, ApJS, 175, 390
Howard S., Keel W. C., Byrd G., Burkey J., 1993, ApJ, 417, 502
Hoyle B. et al., 2011, MNRAS, 415, 3627
Hubble E. P., 1926, ApJ, 64, 321
Hummel E., van der Hulst J. M., Kennicutt R. C., Keel W. C., 1990, A&A, 236, 333
Kauffmann G. et al., 2003, MNRAS, 341, 33
Keel W. C., Kennicutt R. C., Jr, Hummel E., van der Hulst J. M., 1985, AJ, 90, 708
Kennicutt R. C., Jr, Keel W. C., 1984, ApJ, 279, L5
Kennicutt R. C., Jr, Roettiger K. A., Keel W. C., van der Hulst J. M., Hummel E., 1987, AJ, 93, 1011
Lambas D. G., Tissera P. B., Alonso M. S., Coldwell G., 2003, MNRAS, 346, 1189
Larson R. B., Tinsley B. M., 1978, ApJ, 219, 46
Lee G.-H., Park C., Lee M. G., Choi Y.-Y., 2012, ApJ, 745, 125
Li C., Kauffmann G., Heckman T. M., Jing Y. P., White S. D. M., 2008, MNRAS, 385, 1903
Lintott C. J. et al., 2008, MNRAS, 389, 1179
Lintott C. et al., 2011, MNRAS, 410, 166
Lotz J. M., Jonsson P., Cox T. J., Primack J. R., 2008, MNRAS, 391, 1137
Lupton R., Blanton M. R., Fekete G., Hogg D. W., O'Mullane W., Szalay A., Wherry N., 2004, PASP, 116, 133
Masters K. L. et al., 2010, MNRAS, 404, 792
Masters K. L. et al., 2011, MNRAS, 411, 2026
Masters K. L. et al., 2012, MNRAS, 424, 2180
Méndez-Hernández H., Magaña A. M., Hernández-Toledo H. M., Valenzuela O., 2011, Rev. Mex. Astron. Astrofis. Conf. Ser., 40, 78
Moore B., Katz N., Lake G., Dressler A., Oemler A., 1996, Nat, 379, 613
Moore B., Lake G., Katz N., 1998, ApJ, 495, 139
Mullan B. et al., 2011, ApJ, 731, 93
Nair P. B., Abraham R. G., 2010, ApJS, 186, 427
Nakamura O., Fukugita M., Yasuda N., Loveday J., Brinkmann J., Schneider D. P., Shimasaku K., SubbaRao M., 2003, AJ, 125, 1682
Nikolic B., Cullen H., Alexander P., 2004, MNRAS, 355, 874
Noguchi M., 1988, A&A, 203, 259
Patton D. R., Atfield J. E., 2008, ApJ, 685, 235
Patton D. R., Carlberg R. G., Marzke R. O., Pritchet C. J., da Costa L. N., Pellegrini P. S., 2000, ApJ, 536, 153
Patton D. R. et al., 2002, ApJ, 565, 208
Patton D. R., Ellison S. L., Simard L., McConnachie A. W., Mendel J. T., 2011, MNRAS, 412, 591
Perez M. J., Tissera P. B., Lambas D. G., Scannapieco C., 2006, A&A, 449, 23
Pfenniger D., Norman C., 1990, ApJ, 363, 391
Robaina A. R. et al., 2009, ApJ, 704, 324
Romano-Díaz E., Shlosman I., Heller C., Hoffman Y., 2008, ApJ, 687, L13
Salim S. et al., 2007, ApJS, 173, 267
Sandage A., 1961, The Hubble atlas of galaxies. Carnegie Inst., Washington
Schawinski K., Dowlin N., Thomas D., Urry C. M., Edmondson E., 2010, ApJ, 714, L108
Sellwood J. A., Sánchez R. Z., 2010, MNRAS, 404, 1733
Sellwood J. A., Wilkinson A., 1993, Rep. Prog. Phys., 56, 173
Shabala S. S. et al., 2012, MNRAS, 423, 59
Skibba R. A. et al., 2009, MNRAS, 399, 966
Skibba R. A. et al., 2012, MNRAS, 423, 1485
Struck C., 1999, Phys. Rep., 321, 1
Struck C., Dobbs C. L., Hwang J.-S., 2011, MNRAS, 414, 2498
Sundelius B., Thomasson M., Valtonen M. J., Byrd G. G., 1987, A&A, 174, 67
Thomasson M., Donner K. J., Sundelius B., Byrd G. G., Huang T.-Y., Valtonen M. J., 1989, A&A, 211, 25
Toomre A., 1977, in Tinsley B. M., Larson R. B., eds, Evolution of Galaxies and Stellar Populations New Haven. CT: Yale Univ. Observatory, p. 401
Toomre A., Toomre J., 1972, ApJ, 178, 623
Vorontsov-Velyaminov B. A., 1959, Atlas and Catalogue of Interacting Galaxies, Vol. 1. Sternberg Institute, Moscow
Vorontsov-Velyaminov B. A., 1977, A&AS, 28, 1
Xu C. K. et al., 2010, ApJ, 713, 330
Xu C. K., Zhao Y., Scoville N., Capak P., Drory N., Gao Y., 2012, ApJ, 747, 85
York D. G. et al., 2000, AJ, 120, 1579

This paper has been typeset from a TEX/LATEX file prepared by the author.